Facies (2025) 71:19
https://doi.org/10.1007/s10347-025-00709-1

ORIGINAL ARTICLE

Impact of the Paleocene-Eocene thermal maximum on the evolution of larger foraminifera: a new look at an old problem

Victoriano Pujalte[1] · Aitor Payros[1] · Xabier Orue-Etxebarria[1] · Josep Tosquella[2] · Birger Schmitz[3] · Naroa Martínez-Braceras[1]

Received: 15 April 2025 / Accepted: 23 July 2025 / Published online: 11 August 2025

Abstract

A global larger foraminiferal turnover (LFT), first identified in the Pyrenees in 1960, occurred around the Paleocene-Eocene boundary. It is characterized by the replacement of Paleocene assemblages dominated by *Glomalveolina* and *Lockhartia* (west and east Tethys, respectively), with others typified by Eocene *Alveolina* and *Nummulites*. Its relationship with the Paleocene-Eocene Thermal Maximum (PETM), a brief interval of global warming, has been debated at length. This study confirms that the LFT was triggered by the PETM. In the Pyrenean Basin the primary driver of the LFT was the influx of over 100 km^3 of predominantly fine-grained siliciclastic sediment into the sea during the PETM, which disrupted the previous long-lasting oligotrophic conditions. Unlike other K-strategists, *Alveolina* and *Nummulites* adapted to the new ecological conditions, radiating and expanding during the Eocene. Although no comparable siliciclastic influx occurred in the Tethys Ocean, the LFT also coincided with the PETM in Slovenia and Egypt (western Tethys). The link between both events is attributed to adaptations to fluctuating nutrient levels and increased coastal water productivity. In Pakistan and the Himalayas (eastern Tethys), the replacement of Paleocene assemblages appears to have been gradual, leading to the notion that the LFT was not linked with the PETM, but rather resulted from natural evolution. A re-evaluation of the data demonstrates that before the global warming *Alveolina* and *Nummulites* were minor components of the assemblages, but that they rapidly evolved and diversified during the relatively short interval of the PETM, a shift also observed in the Pacific Ocean.

Keywords PETM · Larger foraminiferal turnover · Pyrenean Basin · Tethys Ocean

Introduction: stating the problem

A significant early Paleogene larger foraminifera turnover (LFT) was first reported by Hottinger and Schaub (1960) in the Pyrenees. It was characterized by the rapid diversification of species of a restricted number of genera and a considerable increase in their shell size and adult dimorphism. More specifically, according to data of the Early Paleogene Benthos project (IGCP 286), the main feature of the LFT was the appearance and rapid expansion of large-sized porcelaneous *Alveolina* and of lenticular *Nummulites* (Hottinger 1998; Fig. 1). A diversification of *Assilina* and a few extinctions (e.g., *Miscellanea*) also occurred, but this is less noticeable (Fig. S1A). Building on their discovery, Hottinger and Schaub (1960) established a new stratigraphic stage, termed the Ilerdian. Its stratotype and parastratotype were designated at the Tremp and Campo sections, respectively, in the Spanish provinces of Lerida and Huesca. The base of the Ilerdian Stage was fixed at the LFT (Hottinger and Schaub 1960).

On the other hand, a short-lived global warming event known as the Paleocene–Eocene Thermal Maximum (PETM) occurred 56 million years ago (Ma). This event is recorded in numerous terrestrial and marine sections worldwide by a brief, prominent negative excursion in stable carbon isotopes ($\delta^{13}C$) (McInerney and Wing 2011). The onset of this carbon isotope excursion (CIE), which occurs in the

✉ Aitor Payros
a.payros@ehu.eus

[1] Department of Geology, Faculty of Science and Technology, University of the Basque Country UPV/EHU, Ap. 644, 48080 Bilbao, Spain

[2] Departamento de Ciencias de La Tierra, University of Huelva, Campus Universitario Campus del Carmen, 21071 Huelva, Spain

[3] Department of Physics, University of Lund, P.O. Box 118, 221 00 Lund, Sweden

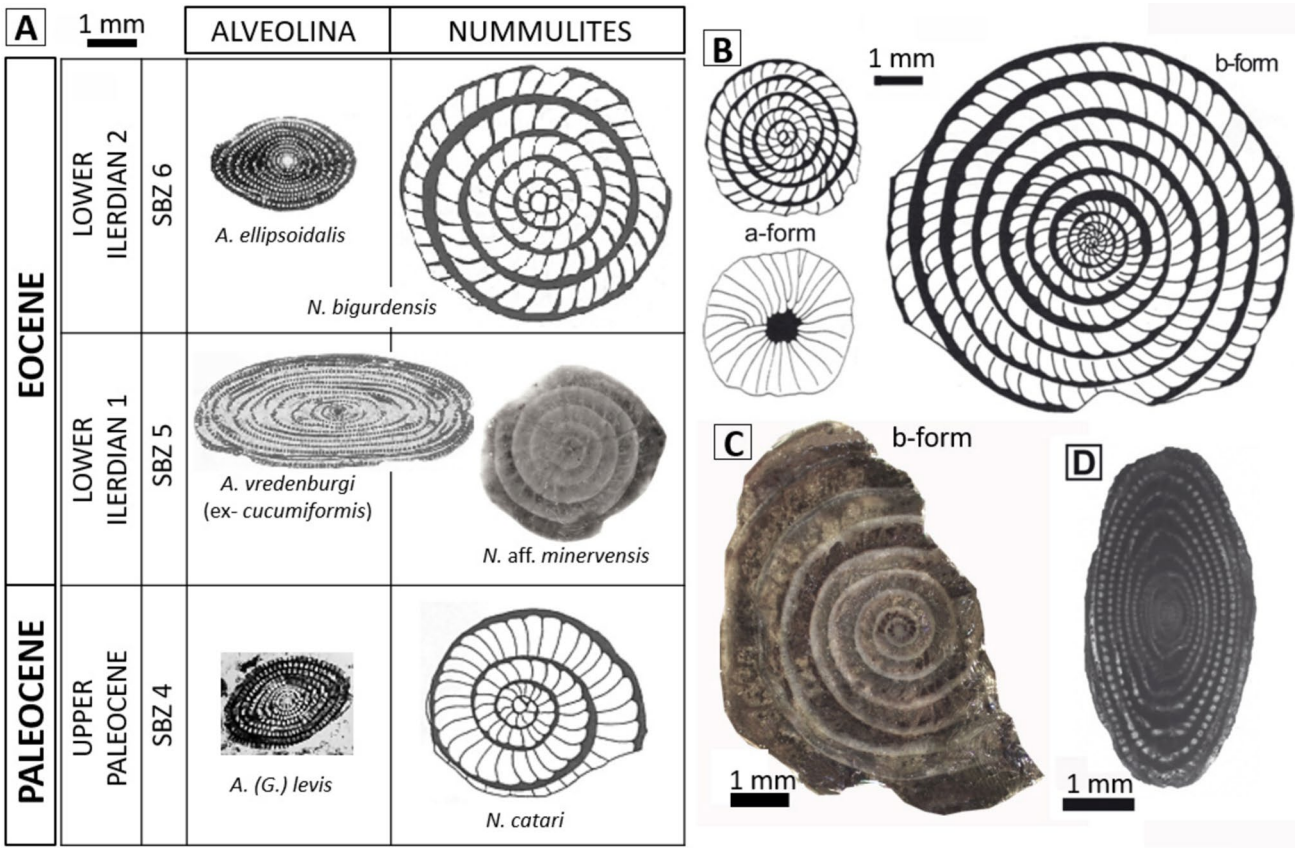

Fig. 1 **A** Chronostratigraphic chart depicting the most representative larger foraminiferal species across the Palaeocene–Eocene boundary, from SBZ 4 to SBZ 6. **B** Line drawings of *Nummulites* aff. *minervensis*, showing an equatorial section and external view of a megalospheric A-form, alongside an equatorial section of a microspheric B-form. **C** Photomicrograph of an equatorial section of a microspheric B-form. **D** Photomicrograph of *Alveolina vredenburgi*

lower part of Chron C24r and at the base of calcareous nannofossil biozone NP10, was designated as the Paleocene-Eocene boundary marker (Aubry et al. 2007). It is now well established that the PETM impacted on a wide range of ecosystems and organisms, including terrestrial mammals (Gingerich 2003) and deep-marine benthic foraminifera (Thomas 2007), caused the extinction and origination of several calcareous nannofossil species (Gibbs et al. 2006) and rapid evolutionary changes in planktonic foraminifera (Kaiho et al. 2006; Petrizzo 2007).

However, the effect of the PETM on larger foraminifera, one of the most prolific calcifying organisms of tropical and mid-latitude carbonate platforms at the time, remains contentious. Hottinger (1998) argued that no connection existed between the two events, asserting that the LFT occurred before the PETM and was the result of evolutionary processes driven by the principles of population genetics. Interestingly, however, this author proposed "*to fix the Paleocene-Eocene boundary in shallow carbonate deposits at the LFT* [an event] *easily recognized in the field with a hand lens.* [Consequently] *all the well-known limestones with larger porcelaneous forms, i.e.* [notably] *alveolinids, and involute nummulitids (s.str.) would fall within the Eocene"* [Hottinger 1998, p. 62]. Ilerdian *Alveolina* and *Nummulites* are, in fact, easily observable even with the naked eye (Figs. S1B, C), and limestones containing these foraminifera are so abundant and conspicuous in the Pyrenees that they have been incorporated into formal stratigraphic terminology (e.g., "Alveolina Limestone Group", Mutti et al. 1988; "Ilerdian Alveolina Limestone Formation", Hamon et al. 2016, and "Alveolina Member", Orue-Etxebarria et al. 2001).

The assertion that the LFT and the PETM were unrelated was primarily based on studies conducted in Campo (Fig. S2). However, subsequent research in this section provided compelling evidence for a temporal correlation between the LFT and the PETM (Orue-Etxebarria et al. 2001; Fig. S2). This correlation was later confirmed in other sections across the southern Pyrenees (discussed below), as well as in sections from Egypt (Scheibner et al. 2005; Scheibner and Speijer 2009; Abd-Elhameed et al. 2023) and Slovenia (Zamagni et al. 2012) in the western Tethys. As a result, the correlation was formally incorporated into the 2012 and

2020 versions of the Paleogene Time Scale (Vandenberghe et al. 2012; Speijer et al. 2020).

However, several recent papers, mostly based on sections from the eastern Tethys and the United Arab Emirates (UAE), contest both the correlation and any causal relationship between the LFT and PETM (e.g., Afzal et al. 2011; Zhang et al. 2013, 2019; Li et al. 2020; Hanif et al; 2021; Kamran et al. 2021; Beasley et al. 2021). Furthermore, Zhang et al. (2013) even oppose using the onset of the CIE/PETM to define the base of the Ilerdian stage.

In order to address the issues raised, this paper has several objectives. Firstly, to present compelling evidence that the LFT and the PETM occurred contemporaneously in the Pyrenean Basin. Secondly, to discuss data supporting a causal relationship between both events. Thirdly, to explore potential explanations for the alleged differing effects of the PETM on larger foraminiferal communities in the UAE and the eastern Tethys. Finally, to advocate for the onset of the CIE/PETM as the primary criterion for defining the base of the Ilerdian Stage.

Database

This contribution primarily draws upon published information. The Pyrenean Basin, where the LFT was discovered, is discussed first, mostly drawing on previous studies conducted by the authors of this article. However, some of their original conclusions have been reassessed in this work, incorporating several new findings. The information about other areas is entirely sourced from the literature, intending a comprehensive overview of current knowledge. By integrating both established research and our own insights, this paper aims to offer a balanced and updated synthesis of key developments in the topic.

The Pyrenean Basin

Setting and palaeogeographic evolution

During Paleocene times the Pyrenean Basin was an east–west elongate marine embayment, opening into the North Atlantic at approximately 35°N (Scotese 2010). The central part of the embayment consisted of a deep-marine trough, named the Basque Basin, which was traversed by an axial deep-sea channel (Fig. 2A). Hemipelagic limestone/marl successions accumulated on the floor of the trough, whereas calcarenites and siliciclastic sands were deposited in the deep-sea channel. The Basque Basin was flanked on both its northern and southern margins by base-of-slope aprons of carbonate breccias and calciturbidites, which originated from adjacent shallow marine carbonate platforms. The carbonate platforms were in turn encircled by subaerial coastal alluvial plains, which in the east were fed from Cretaceous carbonate rocks and in the south from Palaeozoic and lower Triassic siliciclastics of the Ebro Massif (Plaziat 1981; Baceta 1996; Robador 2008; Baceta et al. 2011).

The long-lasting dominance of carbonate sedimentation in the Pyrenean Basin during Paleocene times was abruptly but temporally interrupted during the PETM by a massive influx of siliciclastic sediments (Figs. 2B, 3). Inland, the influx was recorded by the Claret Conglomerate and Yellowish Soils in the Tremp area, which document increased sedimentation rates in the coastal plains (Fig. S3; Schmitz and Pujalte 2003, 2007; Pujalte et al. 2022; Payros et al. 2022). In transitional and marine environments, the influx included significant quantities of quartz sands and pebbly sands (Pujalte et al. 2015, 2016) but was predominantly composed of silty muds (Schmitz et al. 2001). Quartz-rich sands, predominantly sourced from the Ebro Massif, were deposited in valleys incised into the carbonate shelf and their associated braid deltas (Figs. 4–5, S4), as well as in the deep-sea channel. Muds accumulated on the periphery of the braid deltas across the entire carbonate platform and throughout most of the slope, the floor of the Basque Basin and the flanks of the deep-sea channel (Figs. 6, 7, S6–8).

The relationship of these clastic sediments with the PETM is evidenced by carbon isotope profiles ($\delta^{13}C$), as shown in the terrestrial Esplugafreda section and the deep-marine Zumaia section (Fig. S3). In Zumaia, along with many other sections in the Basque Basin, the relationship is further supported by data from planktonic and deep-marine benthic foraminifera, calcareous nannofossils and, in some cases, increased kaolinite concentrations (Table 1). The PETM recovery is recorded in the alluvial deposits of the Tremp area by gypsum-rich deposits, and in marine settings by the resumption of carbonate sedimentation, which persisted into the early Ypresian (Fig. S3).

An accurate calculation of the volume of clastic sediments delivered to the Pyrenean sea during the PETM is hindered by outcrop constraints and Alpine tectonic deformation, which reduced the original width of the Pyrenean Basin. Despite these limitations, a rough estimate indicates that no less than 14 km^3 of sand and approximately 100 km^3 of mud were delivered to the Pyrenean Basin during the PETM (Figs. S8−10). Regardless of the exact volume of the clastic influx, it was sufficient to halt carbonate deposition across the marine area of the Pyrenean Basin during the PETM (Pujalte et al. 1998).

The PETM mudstones from the Ermua, Zumaia and Orio sections reveal that their total organic carbon content ranges from 0.13 to 0.8%, with values reaching up to 30% in carbonaceous remains from Orio (Nuñez-Betelu and Baceta 1994; Pujalte et al. 2015). Additionally, Rock–Eval

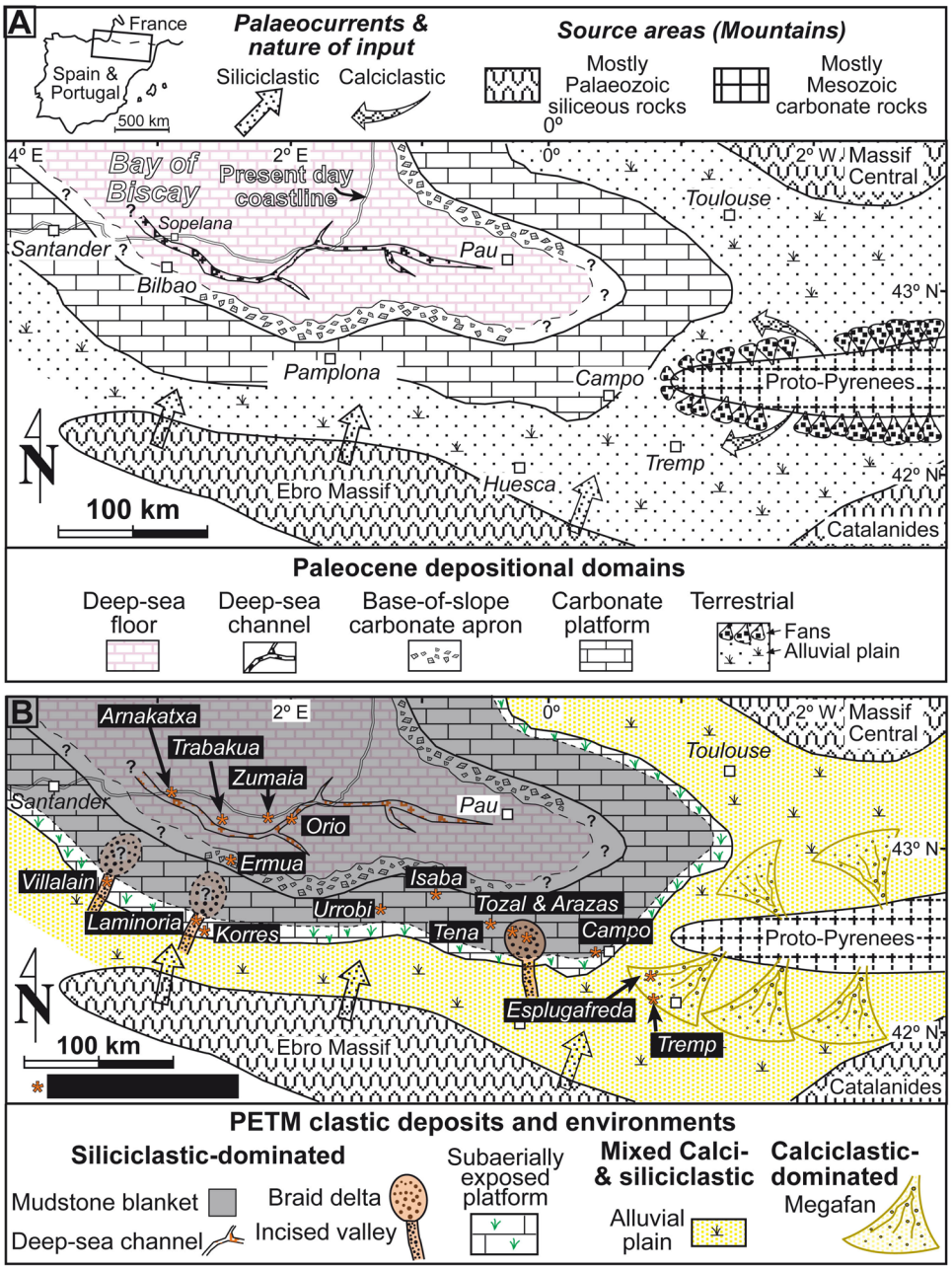

Fig. 2 **A** Pyrenean Basin palaeogeography during Paleocene times. **B** Pyrenean Basin palaeogeography during the PETM interval, with location of reference sections mentioned in the text and Supplementary Figures. Explanation in the text

analyses indicate that this organic carbon is of continental origin (Nuñez-Betelu and Baceta 1994).

Larger foraminiferal changes across the PETM

The distribution of *Alveolina* and *Nummulites* on Paleogene shallow carbonate platforms and ramps was not uniform: the former predominantly occurred on inner platforms with euphotic conditions, whereas the latter thrived on middle platforms characterised by mesophotic conditions, but both coexisted at the inner-middle platform transition (e.g. Martín-Martín et al. 2020; Fig. 3A). This suggests that the presence of these foraminifera in specific sections is determined not only by their age but also by their depositional environment or facies.

This is evident in Paleocene-Eocene sections of the southern Pyrenees, where the PETM allows for a precise tracking (at geological scale) of the lower occurrences of both organisms (Fig. 3B; Table 1). For instance, the first occurrence of *Alveolina* in Tremp (Ilerdian stratotype) is post-PETM and comprises a notably rich assemblage, including *A. dolioliformis*, *A. piper*, *A. globula*, and *A. cucumiformis* (a synonym of *A. vredenburgi*) (Luterbacher 1973; Serra-Kiel et al. 1994). In contrast, in Campo

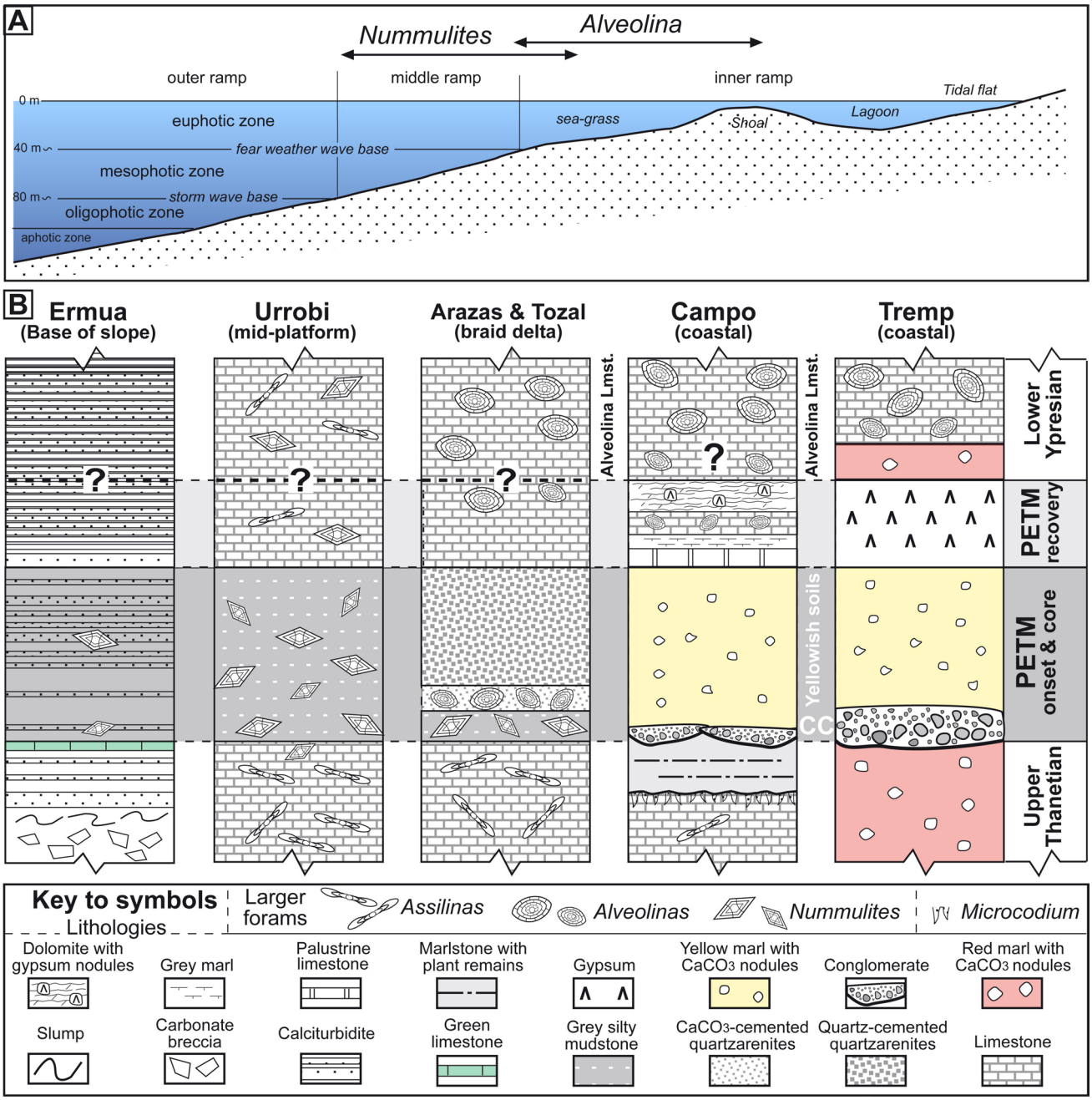

Fig. 3 **A** Environmental distribution of *Alveolina* and *Nummulites* in the lower Eocene successions of Sierra Espuña (SE Spain) (modified from Fig. 9 of Martín-Martín et al. 2020). **B** Synthetic chronostratigraphic panels of representative sections of the Pyrenean Basin, showing the diachronous lower occurrences of *Alveolina* and *Nummulites* across the Paleocene-Eocene boundary interval in different settings

(Ilerdian parastratotype), loose and deformed *Alveolina* sp. appear during the CIE recovery phase, within marls intercalated with dolomitic marls and gypsum (Fig. 3B). In the overlying well-stratified limestones that postdate the PETM, a proliferation of *Alveolina* similar to that of Tremp is observed (Schaub 1973). For descriptive purposes, the proliferation is herein referred to as "radiation."

In the Brecha de Arazas and Tozal del Cebollar sections, *Alveolina* sp. appear in the lower part of the PETM core, predating their occurrence in Tremp and Campo (Figs. 3B, 4). Most specimens of these *Alveolina* occur within tempestites and are therefore resedimented (Fig. 4F, G), although they must have originated from a nearby area.

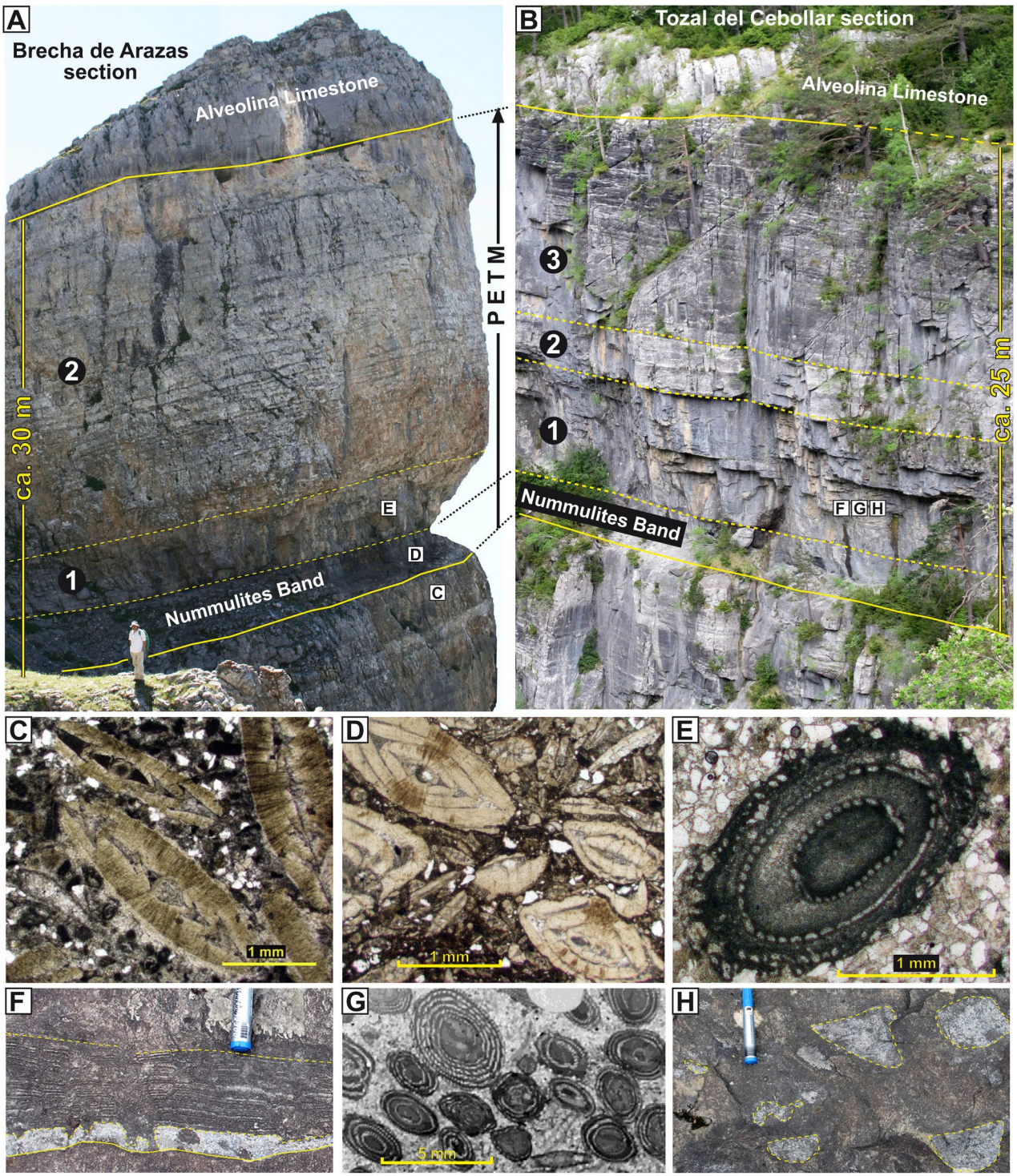

Fig. 4 **A** Field view of the Brecha de Arazas section, Ordesa National Park (modified from Fig. 5 of Pujalte et al. 2016), showing the PETM intervals: Nummulites Band; 1, carbonate-cemented sandstone with *Alveolina*; 2, coarsening-up quartz-cemented sandstone and pebbly sandstone. **B** Field view of the Tozal del Cebollar section, Ordesa National Park (modified from Fig. 14 of Pujalte et al. 2016), showing the PETM intervals: Nummulites Band; 1, carbonate-cemented sandstone with *Alveolina*-rich tempestites and "pockets"; 2, carbonate-cemented sandstone with whitish streaks rich in resedimented larger foraminifera (undetermined); 3, coarsening-up, parallel-laminated quartz-cemented sandstone and pebbly sandstone. **C, D, E** Thin-section photomicrographs showing *Assilina*, *Nummulites*, and *Alveolina*, respectively, from the Brecha de Arazas section (location of samples in A). **F** Close-up of a tempestite from the Tozal del Cebollar section, composed of a lag of *Alveolina* in its lower part and parallel-laminated sandstone, with scape galleries, in its upper part. **G** Thin-section photomicrograph of the lower part of a tempestite, showing numerous *Alveolina*, with their imbrication indicating traction currents. **H** Examples of *Alveolina*-rich "pockets," probably resulting from bioturbation of tempestites

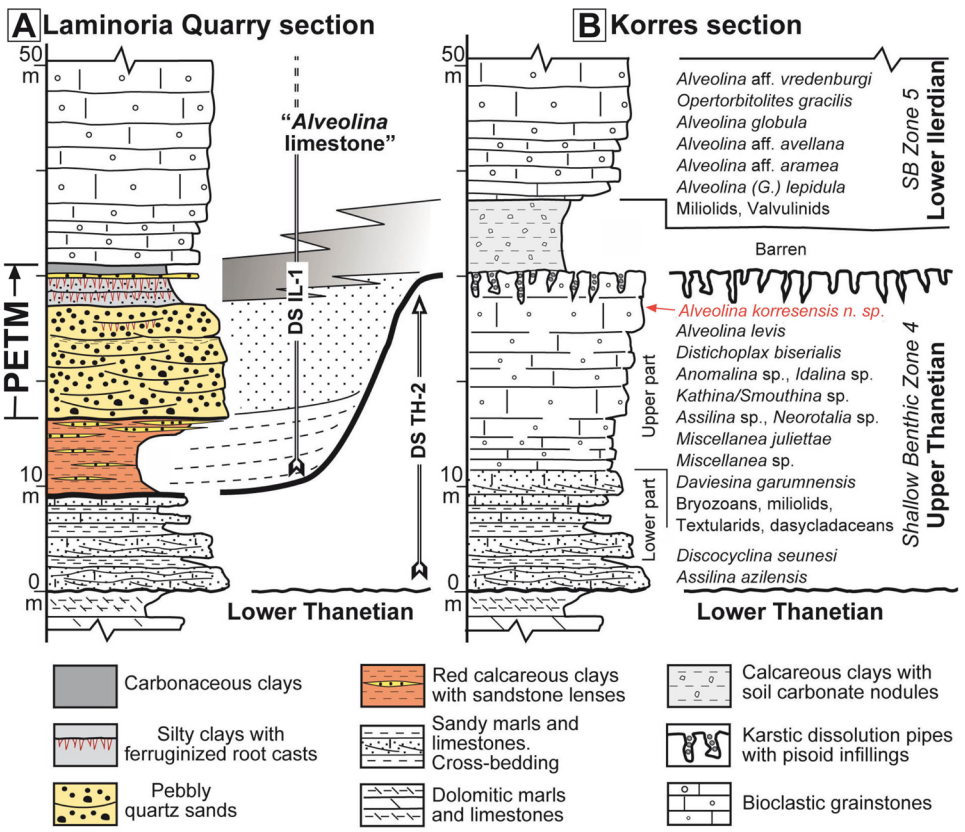

Fig. 5 Lithological log and larger benthic foraminifera of the Korres section (slightly modified from Fig. 4 of Pujalte et al. 2015)

Serra-Kiel et al. (2020) reported an even earlier appearance of *Alveolina* in Korres, with a new species (*A. korresensis*) which occurs just below the karstified surface capping the upper Thanetian limestones (Fig. 5). It is important to note that, to date, this species has not been identified in any other section, suggesting that its appearance was highly localised.

During the PETM, *Nummulites* were abundant in middle platform areas but absent from inner and outer platforms (e.g., Korres and Isaba, Figs. 5, S5B; Table 1). The most significant middle platform section studied is Urrobi, which was sampled at high resolution (Pujalte et al. 2003; Fig. 6). The samples from most of the upper Thanetian limestones comprise two types of *Assilina*, plus local operculiniform *Nummulites* (probably, *N. catari*), a typical association of zone SBZ4 (Fig. 6B, C). However, a few specimens of lenticular *Nummulites* appear in the uppermost part of these limestones (Fig. 6D), representing the lowest occurrence of these organisms in this section and, to our knowledge, in the Pyrenees and the Tethys Ocean. The Thanetian limestones are concordantly overlain by a 0.9-m-thick interval of PETM mudstones, which contains a markedly different assemblage dominated by a single species of *Nummulites* (*N.* aff. *minervensis*, sensu Schaub 1981, comprising 60–80% of the foraminiferal population). Accordingly, this interval was referred to as the Nummulites Band (Pujalte et al. 2003; NB in Fig. 6B). The population is largely composed of A-forms, which originate through asexual reproduction from either larger B-forms or other A-forms. Adult larger specimens are sparse and diminutive within the lower 10–15 cm of the Nummulites Band but increase both in abundance and size upwards. Interestingly, Hottinger (1998, p. 63) concluded that "*shorter-lived gamonts and/or schizonts, produced by asexual reproduction, exploit by their accelerate initial growth the maxima of nutrient input, forming spring and autumn blooms*". In the limestones overlying the Nummulites Band, which belong to biozone SBZ5, the foraminiferal assemblage becomes progressively more diverse (Fig. 6B).

The PETM is also recorded by a *Nummulites*-rich muddy interval similar to the Nummulites Band in the Brecha de Arazas and Tozal del Cebollar sections, both in the Ordesa and Monte Perdido National Park (Figs. 4A, B; Table 1). This Nummulites Band occurs along the so-called Faja de las Flores ledge, a striking 3-km-long trail carved into a near-vertical carbonate cliff formed by the differential erosion of PETM mudstones (Figs. S8B, C). In fact, it can be traced on maps as far as the Tena section, located 17 km to the west (Fig. S5A), where nearly all the larger foraminifera from the Nummulites Band were identified as *N. aff. minervensis* (Robador et al. 1991). The *Nummulites* from the Brecha de Arazas and Tozal del Cebollar sections remain to be determined, but given their morphological similarity, they

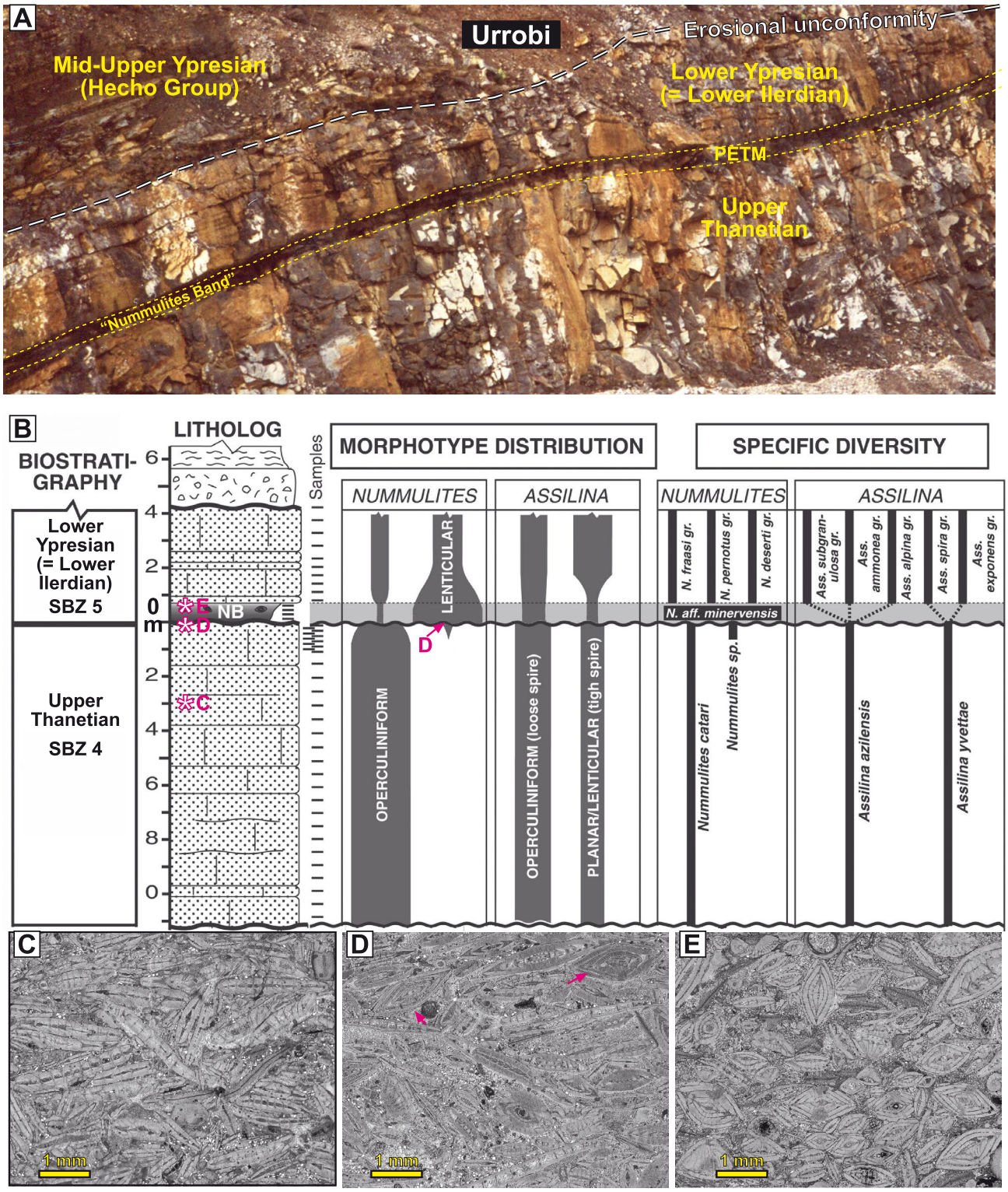

Fig. 6 **A** Field view of the Urrobi section, showing the PETM mudstones of the Nummulites Band interbedded between upper Thanetian and lower Ypresian carbonates. **B** Litholog with nummulitid morphotype distribution and specific diversity observed in thin sections of close-spaced samples (slightly modified from Pujalte et al. 2003, Fig. 3). Asterisks show the location of samples **C**–**E**. **C** Assemblage composed of lenticular ("true") *Assilina*, operculiniform *Assilina* and operculiniform *Nummulites*. **D** Similar to C, but with scattered specimens of lenticular *Nummulites* (arrowed). **E** Assemblage dominated by A-forms of lenticular *Nummulites* in a sample from the Nummulites Band (NB)

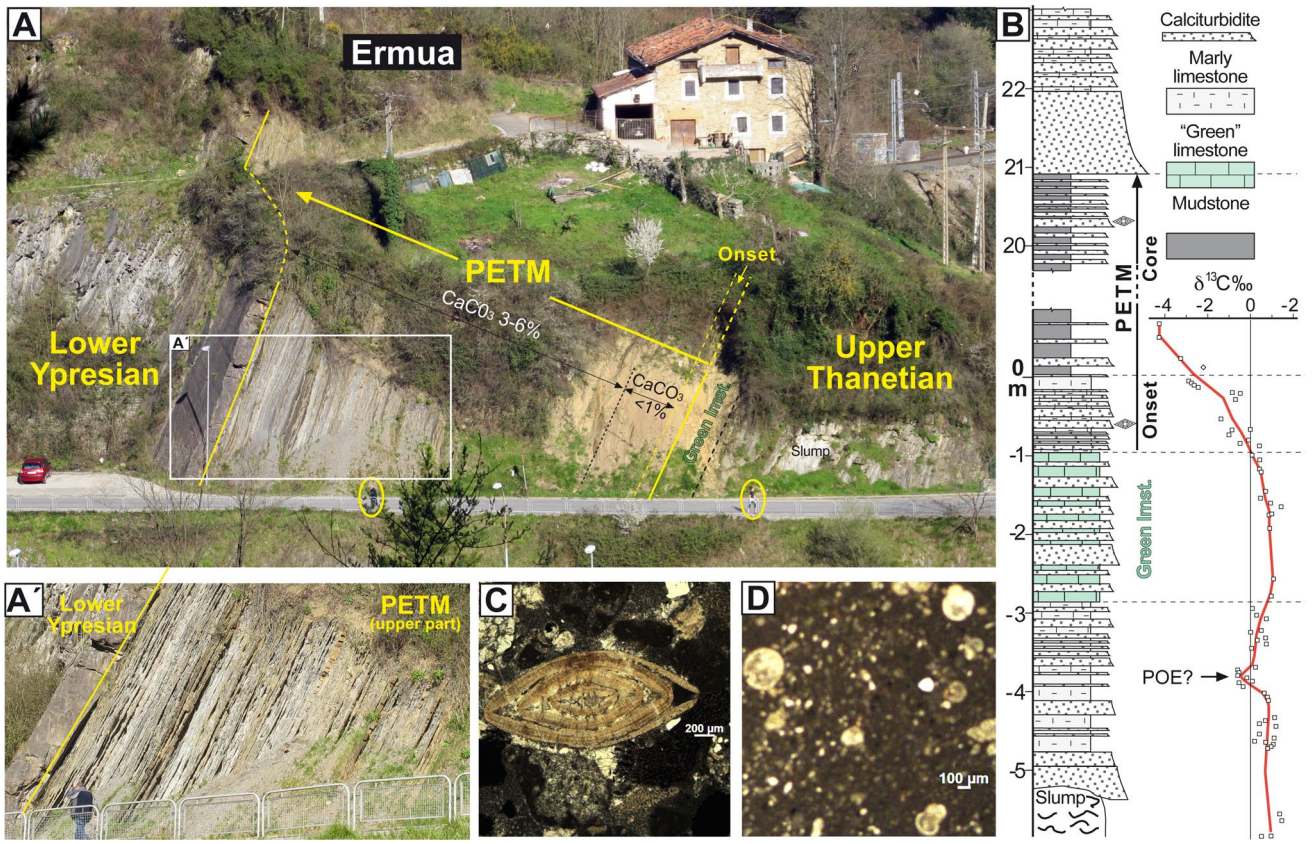

Fig. 7 **A** Field view of the base-of-slope Ermua section. **A´** Close-up of the upper part of the PETM interval showing numerous calciturbidites. **B** Litholog of the section with inorganic carbon isotopic profile (modified from Schmitz et al. 2001, Fig. 4B) and the location of calciturbidites containing lenticular *Nummulites* (diamonds). **C** Lenticular *Nummulites* from a calciturbidite at the PETM onset. **D** Photomicrograph of the topmost Thanetian "Green limestone", a wackestone with planktonic foraminifera

are likely to predominantly belong to the same species. This suggests that the sudden proliferation of *N. aff. minervensis* was not confined to the Urrobi section but was, in fact, a widespread phenomenon across the middle platform.

In the base of slope Ermua section the PETM muds contain numerous fine-grained and several medium-grained bioclastic calciturbidites up to 10 cm thick (Figs. 7A, B). The latter contain *Nummulites*, arguably derived from the middle platform (Figs. 7C).

Larger foraminiferal changes across the PETM in the Tethys Ocean

In the western Tethys (Fig. 8A), the relationship between the PETM and the LFT was analysed in Slovenia (Zamagni et al. 2012) and on the Galala Plateau in Egypt (Scheibner et al. 2007; Scheibner and Speijer 2009; Abd-Elhameed et al. 2023). These studies concluded that both events were coeval and occurred at the SBZ4/5 boundary, in line with the Pyrenean findings.

Contrarily, Beasley et al. (2021) challenged this relationship using data from a borehole in the UAE (Fig. 8B). However, it is important to note that the Paleocene-Eocene boundary interval in this borehole is incomplete. The onset of the PETM is recorded in a 4 m-thick segment, within which no larger foraminiferal changes were observed. This segment is bounded below and above by two core gaps with durations of 300 kyr and 1.5 Myr, respectively (Fig. 8B). The upper gap spans the entirety of the PETM core and recovery, as well as part of the early Ypresian. The foraminiferal assemblage in the strata above this gap differs from that of the Thanetian, indicating that significant changes must have occurred during the 1.5 Myr missing interval. This renders the borehole unsuitable for addressing the issue under consideration.

Results from the eastern Tethys are somewhat inconsistent. For instance, a recent study from Baroch Nala in Pakistan (Ali et al. 2025) constrained the PETM using inorganic and organic carbon isotopes, along with other proxy data. The study found that *Nummulites*, and less commonly *Alveolina*, appeared during the core and recovery of the PETM, although their precise locations were not specified. After the

Table 1 Lithologies and first occurrences of *Alveolina* and *Nummulites* across the Paleocene-Eocene interval in the Pyrenean Basin

Section, Setting	PETM indicators	Dominant Lithologies	First Occurrences	References
Esplugafreda, Alluvial	CIE ($\delta^{13}C$ profile), Kaolinite influx	Post PETM: mudstone PETM recovery: gypsum PETM core: conglomerates & mudstone	No larger foraminifera	Schmitz & Pujalte (2003, 2007), Manners et al. (2013)
Tremp, Coastal	CIE ($\delta^{13}C$ profile)	Post PETM: marls & limestones PETM recovery: gypsum PETM core: conglomerates & mudstone	*Alveolina* radiation No larger foraminifera	Serra-Kiel et al. (1994), Schmitz & Pujalte (2007), Manners et al. (2013), Pujalte et al. (2022), Payros et al. (2022)
Campo, Coastal	CIE ($\delta^{13}C$ profile), Calc. nannofossils, Planktonic forams, Magnetostratigraphy	PETM recovery: limestones, dolomite & gypsum PETM core: congl. & mudstones	*Alveolina* No larger foraminifera	Schaub (1973), Orue-Etxebarria et al. (2001), Schmitz & Pujalte (2003), Pujalte et al. (2009)
Laminoria, Incised valley	CIE ($\delta^{13}C$ profile), Kaolinite influx	Post PETM: limestones PETM core: sands	*Alveolina* radiation No larger foraminifera	Pujalte et al. (2015)
Korres, Inner platform	PETM not recorded	Post PETM: limestones U. Thanetian: limestones	*Alveolina* radiation *Alveolina*	Pujalte et al. (2015), Serra-Kiel et al. (2020)
Brecha Arazas & T. Cebollar Braid delta	CIE ($\delta^{13}C$ profiles)	PETM core: sandstones PETM core: mudstones	Alveolina *Nummulites*	Pujalte et al. (2016)
Tena, Middle platfom	Correlation with T. del Cebollar section	Post PETM: limestones PETM core: Mudstones	*Alveolina* radiation *Nummulites*	Robador et al. (1991), Serra-Kiel et al. (2020)
Urrobi, Middle platfom	CIE ($\delta^{13}C$ profile), Planktonic forams	PETM core: mudstones U. Thanetian: limestones	*Nummulites* *Nummulites*	Pujalte et al. (2003), Serra-Kiel et al. (2020)
Isaba, Outer platfom	Calc. nannofossils, Planktonic forams	PETM core: mudstones	No larger foram	Pujalte et al. (2003), Serra-Kiel et al. (2020)
Ermua, Base-of-slope	CIE ($\delta^{13}C$ profile), Calc. nannofossils, Planktonic forams	PETM onset & core: mudstones and calciturbidites	*Nummulites* (resedimented)	Orue-Etxebarria et al. (1996), Bolle et al. (1998), Schmitz et al. (2001), Serra-Kiel et al. (2020)
Zumaia, Deep marine	CIE ($\delta^{13}C$ profile), Calc. nannofossils, Planktonic and deep marine benthic foraminifera, Magnetostratigraphy	PETM recovery: marls & limestones PETM core: mudstones	No larger forams	Schmitz et al. (1997a), Orue-Etxebarria et al. (2004), Dinarès-Turell et al. (2002), Alegret et al. (2009), Storme et al. (2012)
Trabakua east & Arnakatxa, Deep marine	Calc. nannofossils, Planktonic forams, Correlation	PETM core: mudstones	No larger forams	Orue-Etxebarria et al. (1996), Martínez-Braceras et al. (2023)
Orio, Deep-sea channel	CIE ($\delta^{13}C$ profile), Kaolinite influx	PETM core: sandstones and pebbly sandstones	No larger forams	Pujalte et al. (2015)

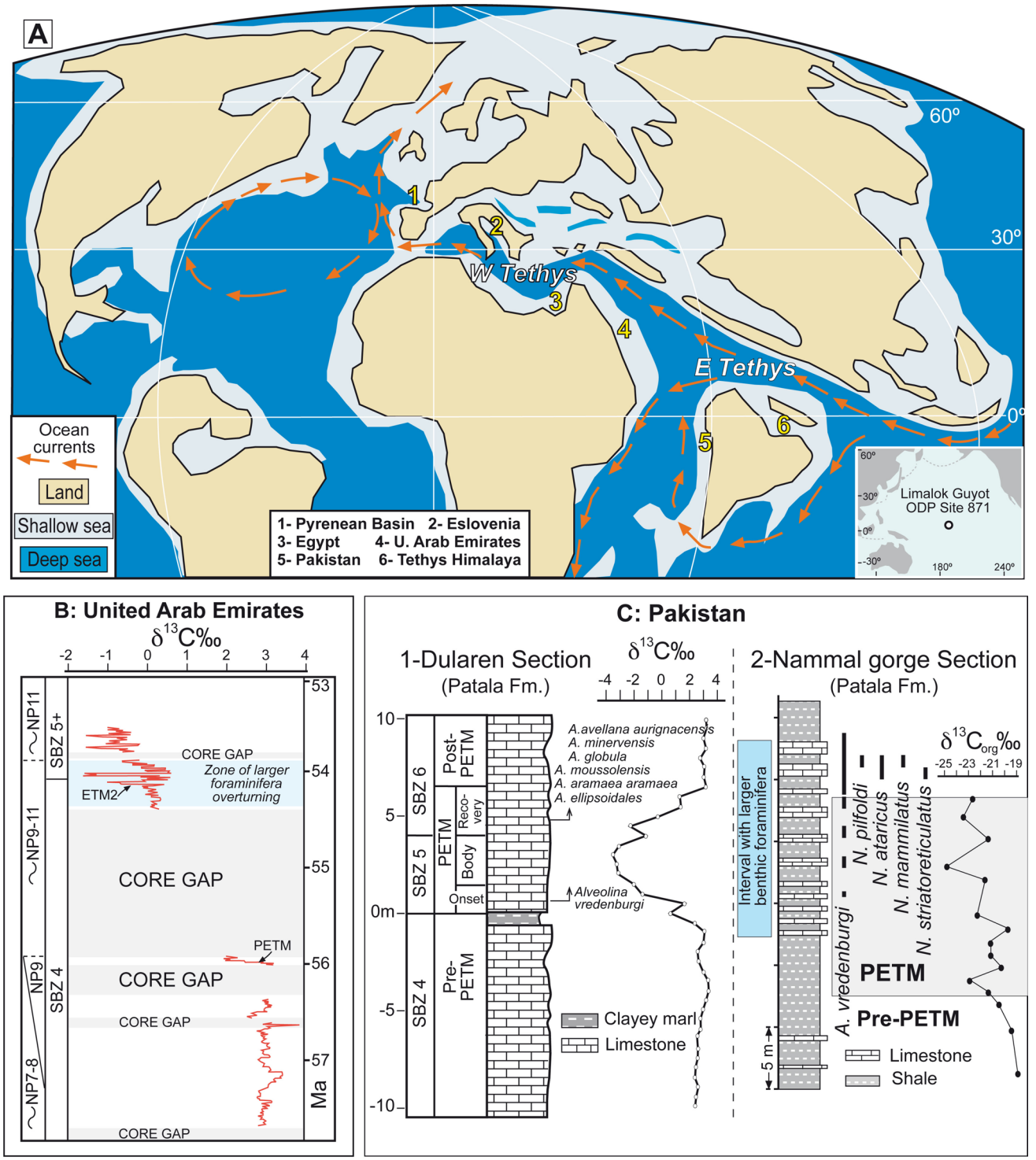

Fig. 8 **A** Global palaeogeographic map for 56 Ma (modified from Scotese 2010), with location of areas considered in the text. Oceanic currents adapted from Fig. 1 of Haq (1981). The inset in the lower right corner shows the present-day location of the Limalok Guyot in the Pacific Ocean (ODP Site 871). **B** Carbon isotope data from a borehole of the United Arab Emirates, with calcareous nannofossils and SBZ zonations; note extensive core gaps (simplified from Fig. 7 of Beasley et al. 2021). **C** Lithologs, isotope profiles, SBZ zonations and range of *Alveolina* and *Nummulites* in two sections of Pakistan (Dularen, modified from Fig. 6 of Kamra et al. 2021; Nammal gorge, modified from Fig. 5 of Hanif et al. 2020)

PETM, *Nummulites* and *Assilina* dominated the assemblage, *Alveolina* becoming increasingly frequent. These findings are not at odds with those from the Pyrenees and the western Tethys.

However, other studies reached different conclusions. According to Afzal et al. (2011), for instance, late Paleocene larger foraminiferal assemblages in the Indus Basin are taxonomically comparable to those in the western Tethys. Contrarily, the earliest Eocene assemblages lack typical western Tethys *Nummulites*, and *Alveolina* occurrences are sparse. The authors attributed this to possible biogeographical barriers, potentially arising from the early stages of the India-Asia collision. Afzal et al. (2011) did not conclusively constrain the CIE/PETM due to limited sampling resolution. Consequently, they placed the base of the Eocene at the first appearance of *Alveolina* sp.

In the Dularen section of the Potwar Basin (Pakistan), the onset of the PETM is characterised by an approximately 5‰ CIE (Kamran et al. 2021; Fig. 8C). Although no significant larger foraminiferal changes occur, it is noteworthy that *A. vredenburgi* first appears during the onset of the CIE. Kamran et al. (2021) observed a more prominent shift in the foraminiferal assemblage during the recovery of the PETM, which included the emergence of six *Alveolina* species and two *Nummulites* species (Fig. 8C). They correlated this shift with the Larger Foraminiferal Extinction and Origination (LFEO) event originally described by Zhang et al. (2013) in the Tethys Himalaya (discussed below).

Similarly, in the Nammal Gorge section of the Salt Range (Pakistan), Hanif et al. (2021) reported a transition from a typical Paleocene larger foraminiferal assemblage to another dominated by *Alveolina* (including *A. vredenburgi*), *Nummulites* and *Assilina*. Most likely, by "typical Paleocene assemblage" the authors referred to one dominated by *Lockhartia*, which justifies the term "Lockhartia Sea" used by Hottinger (1998) and Bassi (2014). They suggested that this shift approximately corresponds to the LFT, as the first occurrence of *A. vredenburgi* is observed around the middle of the PETM (Fig. 8C). It should be noted, however, that larger foraminifera are only present in a limited portion of this section (Fig. 8C).

In the Tethys Himalaya, middle Paleocene to lower Eocene carbonates are predominantly preserved in three distinct outliers (Fig. 9A). Research conducted at Tingri and Gamba by Zhang et al. (2013, 2019) and Li et al. (2017, 2020) highlighted several differences when compared to the Pyrenees and the western Tethys, the most striking being the presence of *Alveolina* in upper Thanetian deposits (Fig. 9B).

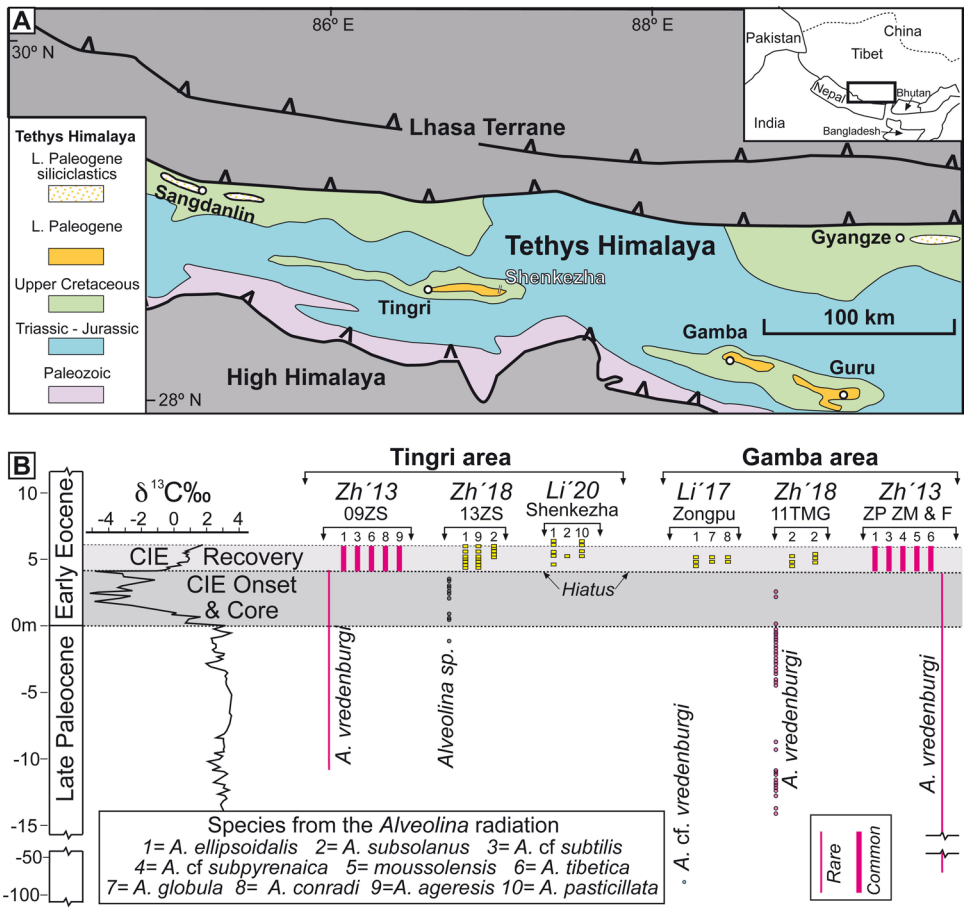

Fig. 9 **A** Simplified outcrop map of south Tibet with indication of localities and sections mentioned in the text (modified from Fig. 1 of Zhang et al. 2019). **B** Vertical distribution of *Alveolina* species in representative sections of the Tingri and Gamba (isotopic curve from Zhang et al. 2013, Fig. 3; *Alveolina* data from: ZH´13, Zhang et al. 2013; ZH´19, Zhang et al. 2019; Li´17, Li et al. 2017; Li´20, Li et al. 2020)

However, these occurrences are irregularly distributed. At Gamba, *A. vredenburgi* is found approximately 65 m below the PETM onset in sections ZP, ZM and F, but only about 15 m below the PETM onset in Section 11 TMG. An even older occurrence of *A. cf. vredenburgi* was identified in a single sample located around 100 m below the CIE in the Zongpu section at Gamba. At Tingri, *A. vredenburgi* appears 11 m below the PETM in Section 09ZS, while a single occurrence of *Alveolina* sp. is reported just under the PETM in Section 13ZS (Fig. 9B). In contrast, no *Alveolina* were detected below the PETM in the Shenkezha section at Tingri (Fig. 9B).

Zhang et al. (2013) were the first to report a significant foraminiferal extinction and origination event (LFEO) during the CIE recovery in the Tethys Himalaya. This event was characterised by the disappearance of several typical Paleocene genera, alongside the initial dominance of *Alveolina* (Figs. 9B, 10A,B). Thus, Paleocene *Alveolina* specimens

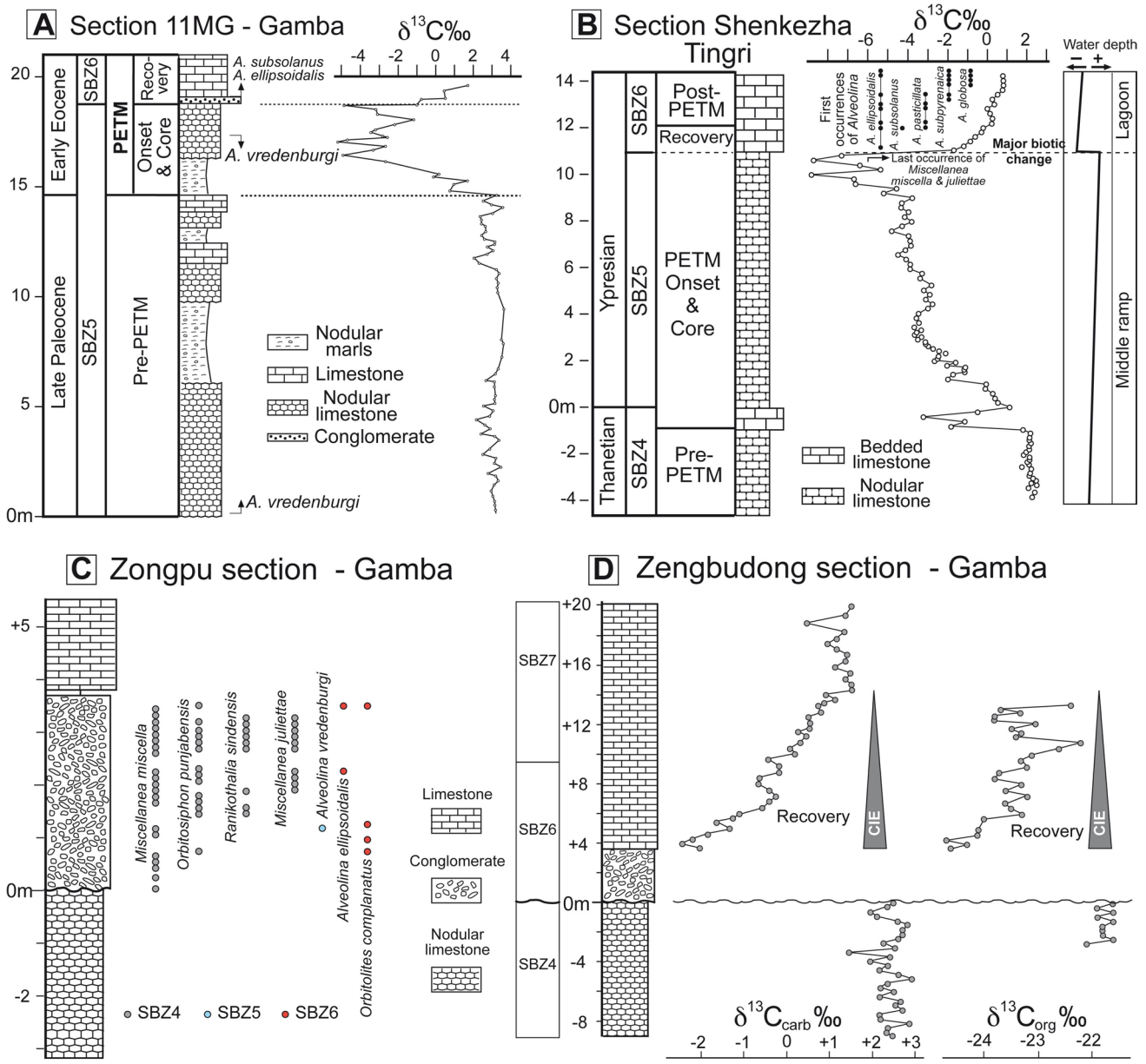

Fig. 10 **A, B** Lithologs, isotope profiles, SBZ zonations and range of selected larger foraminifera in two sections of the Tethys Himalaya (11MG at Gamba, modified from Fig. 4 of Zhang et al. 2019; Shekezha, modified from figs. 3 and 4 of Li et al. 2020). **C** Lithological log of the Zongpu section (Gamba area) across the Paleocene-Eocene boundary, with distribution of larger foraminifera in carbonate clasts of the conglomerate bed (modified from Fig. 3 of Li et al. 2017). **D** δ.^{13}C curves for whole-rock carbonate and organic matter from the Zengbudong section, Gamba area (modified from Fig. 7 of Li et al. 2017)

belong to one single species, only occur in low numbers in some sections, and are absent in others (Fig. 9B). In contrast, *Alveolina* became more common and diversified during the CIE recovery in all Sections (10 different species, Fig. 9B), serving as the main evidence of the LFEO. Zhang et al. (2013, 2019) tentatively attributed the LFEO to a eutrophication event triggered by intensified continental weathering during the CIE recovery, but no sedimentological evidence was provided.

Li et al. (2017), also studying the Tibetan Himalaya, discovered an erosional disconformity near the Paleocene–Eocene boundary that they claim can be traced for approximately 200 km across southern Tibet. At the Zongpu section in Gamba, the disconformity is overlain by a channel-like conglomerate approximately 3.5 m thick, composed of intraformational carbonate clasts (Fig. 10C). Most clasts contain larger foraminifera from biozone SBZ4, but a few include *A. vredenburgi* and *A. ellipsoidalis*, and are attributed to SBZ5 and SBZ6, respectively (Fig. 10C). Inorganic and organic carbon isotope profiles from the Zengbudong section indicate that only the recovery phase of the PETM is preserved (Fig. 10D). Taken together, these data demonstrate that the unconformity involves a hiatus spanning the upper part of the Thanetian and the onset and core of the PETM. Zhang et al. (2019) and Li et al. (2020) identified correlative hiatuses in other sections of Gamba and Tingri, located at or near the transition between the core and recovery of the PETM. However, these were of lesser magnitude, as they partly preserved the PETM onset and core (Figs. 10A, B).

In the Shenkezha section (Tingri area), Li et al. (2020) documented species extinctions and originations during the PETM recovery associated with the LFEO (Fig. 10B). However, unlike Zhang et al. (2013, 2019), rather than to eutrophication, they attributed these taxonomic changes to an environmental shift from a middle-ramp to a lagoonal setting, driven by a relative sea-level fall. Evidence for this sea-level fall includes the widespread disconformity at Zengbudong, which is also present at Shenkezha. Consequently, they concluded that the fundamental biotic changes during the PETM recovery were primarily driven by fluctuations in relative sea level.

Arguing that *A. vredenburgi* is a key marker of the early Ilerdian biozone SBZ5, Zhang et al. (2013, 2019) concluded that the P–E boundary, as marked by the onset of the CIE/PETM, is not located at the SBZ4/5 boundary in Tibet but rather in the upper part of SBZ5 (Fig. 10A). As such, they assert that in the Himalayas the LFT is neither contemporaneous with, nor related to, the PETM. In doing so, they align with Hottinger (1998) in attributing the LFT to natural evolutionary processes. Furthermore, Zhang et al. (2013) argued against placing the base of the Ilerdian at the onset of the PETM, as the establishment of this stage was originally based on the evolution of larger foraminifera. Consequently, they position the base of the Ilerdian at the earliest occurrence of *A. vredenburgi*.

Larger foraminiferal changes across the PETM in the Limalok Guyot (Pacific Ocean)

The Limalok Guyot (Pacific Ocean) was drilled at ODP Site 871 (Fig. 8A), yielding several pieces of evidence that complement the findings from the Pyrenees and the Tethys. The guyot, formed on a volcanic edifice, comprises approximately 290 m of lower Paleocene to middle Eocene platform carbonates, age-dated with *Alveolina* and *Nummulites* (Nicora et al. 1995). The guyot was located at a palaeolatitude of ~ 11°S in the late Paleocene and was drowned in the middle Eocene at ~ 8°S (Premoli Silva et al. 1993). As noted by Robinson (2011), its isolation allows for the investigation, free from the influence of continental margins, of the effects of changes in surface ocean temperature and chemistry caused by the PETM on a shallow-water carbonate succession.

Of the 40 cores recovered, 29 were composed of shallow-marine carbonates (Fig. 11). The analyses of carbon isotopes from bulk samples generally yielded positive $\delta^{13}C$ values, most ranging between + 1.5 and + 2.5‰ in the lower part of the borehole but declining upwards (Robinson 2011). Superimposed on this general trend, a negative excursion of up to ~ 3‰ was observed in several samples at ~ 336 mbsf (core 23R, Fig. 11). Nicora et al. (1995) identified *Nummulites* in overlying cores, including *N. deserti* in core 21R. This species is characteristic of the SBZ5 and SBZ6 biozones (Fig. S1A), providing biostratigraphic evidence that the CIE at core 23R corresponds to the onset of the PETM. The distribution of *Alveolina*, also present in the borehole, is particularly noteworthy. Single specimens of *Alveolina* sp. were observed in cores 25R and 26R, situated approximately 34 and 35 m below the onset of the CIE/PETM, respectively (Fig. 11). However, *Alveolina* becomes abundant in core 20R and very abundant in core 19R, above the PETM (inset in Fig. 11), a distribution similar to that observed in the Tethys Himalaya (cf. Figure 9B).

A notable feature of this guyot is the absence of any significant interruption in carbonate production during the PETM interval. According to Robinson (2011), the continuity in carbonate sedimentation suggests either that the duration of the PETM acidification was below the resolution of the record or that its intensity was insufficient to cause any noticeable effects. As a result, Robinson (2011) concluded that a decrease in surface water pH lasting more than 10 kyr was unlikely.

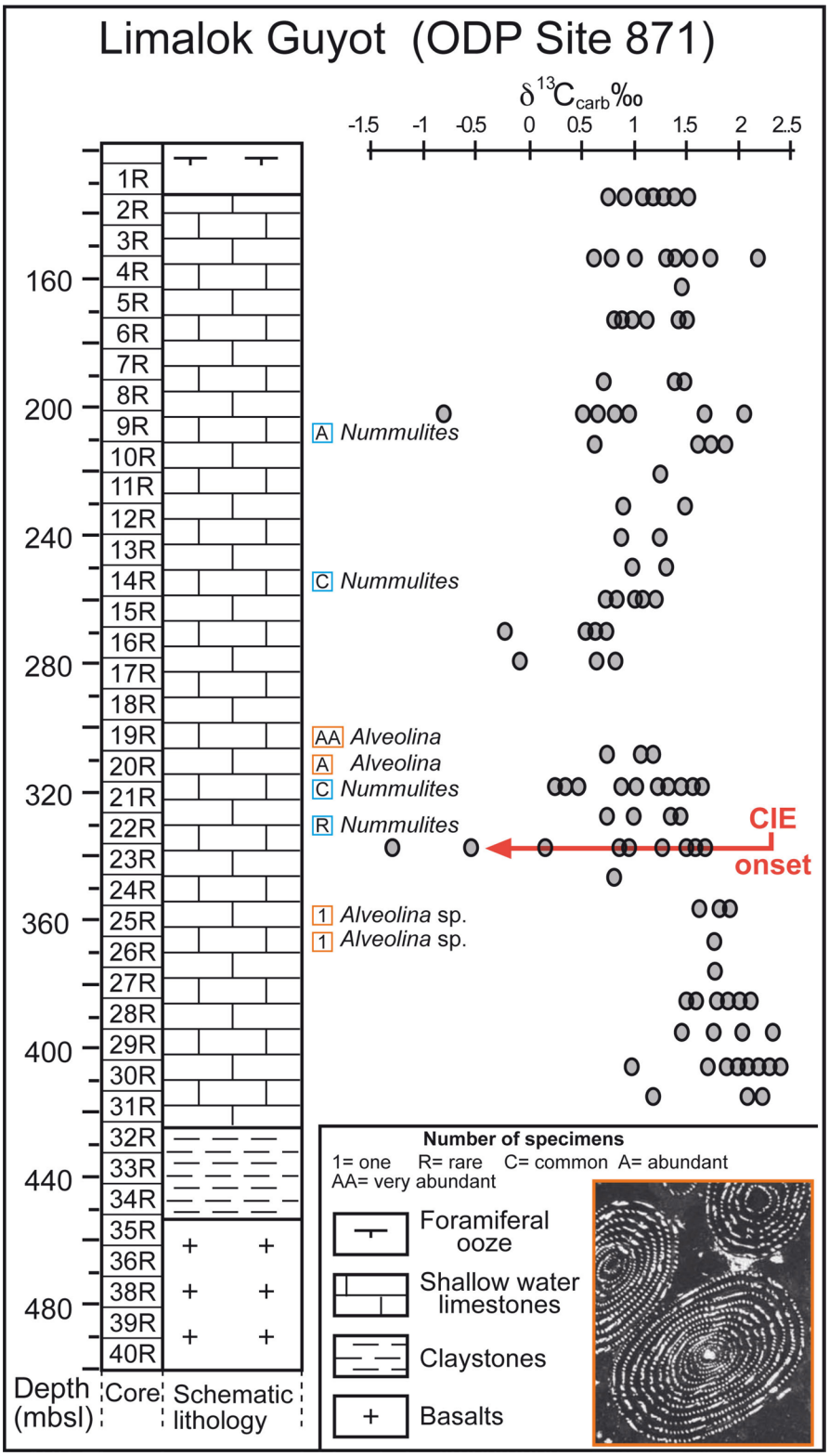

Fig. 11 Lithostratigraphy and $\delta.^{13}C$ isotope data (grey dots) of ODP Hole 871C at the Limalok Guyot, Pacific Ocean (modified from Fig. 1 of Robinson 2011). *Alveolina* and *Nummulites* data from Table 1 of Nicora et al. (1995). The inset in the lower right corner illustrates slightly oblique axial sections of *Alveolina* (*Alveolina*) sp. aff. *A. sakaryaensis* from Core 19R (slightly modified from image 7, plate 2, of Nicora et al. 1995)

Discussion

Impact of the PETM on larger foraminifera in the Pyrenean Basin

Two key facts must be taken into account (Fig. 3B, Table 1): (1) the diachronous lower appearances of *Alveolina* and *Nummulites* in sections from different settings and

(2) the significant influx of mostly fine-grained siliciclastic sediments during the onset and core of the PETM.

The apparent diachrony is clearly an artefact of the important early Ilerdian sea-level rise in the Pyrenean Basin, which caused a time-transgressive displacement of the euphotic and mesophotic environments inhabited by *Alveolina* and *Nummulites*, respectively. A clear proof of this rise is the displacement of the shoreline, which broadly coincides with the transition from continental red mudstones to shallow-marine limestones. In the Campo-Tremp transect, for example, the shoreline advanced landward by as much as 150 km during the early Ilerdian (Baceta et al. 2004, their Fig. 3.46). The sea-level rise is also evident in individual sections. For example, in Campo it is recorded by the vertical facies stacking above the subaerial exposure capping the Navarri Formation (Fig. S2): continental siliciclastics (Mb 1); palustrine/lagoonal limestones with *Alveolina* (Mb 2a); inner platform *Alveolina* limestone (Mb 2b); open-marine limestones with *Nummulites* (Mb 2c); alternations of marls/marly limestones with planktonic foraminifera (Mb 3). Consequently, to accurately monitor the evolution of larger foraminifera in any basin, it is crucial to study sections from diverse depositional settings.

An additional effect of sea-level changes in carbonate platforms is the development of discontinuities, which have been routinely used to delimit depositional sequences and parasequences (Van Wagoner et al. 1988). Luterbacher (1998) highlighted the possibility that certain compositional changes in foraminiferal assemblages in vertical sections may, in fact, be associated with discontinuities, referring to this phenomenon as "telescoping" (Fig. 12A).

The temporal coincidence between the PETM and the LFT in the Pyrenees suggests a causal relationship. It is well-established that the PETM led to seawater acidification, a rise in ocean temperatures, and changes in terrestrial runoff (McInerney and Wing 2011). The acidification caused extensive dissolution of deep-ocean carbonates (Zachos et al. 2005), although it was less significant in shallower waters. In fact, the vast majority of shallow-marine carbonates from the Tethys show no evidence of dissolution across the Palaeocene–Eocene boundary (e.g., Figs. 8C, 9). Data from the Limalok Guyot further support this notion. It is reasonable to infer that seawater acidification in shallow-marine environments during the PETM was minimal and, consequently, had little to no impact on larger foraminifera. The same holds true for the rise in seawater temperatures, as these organisms thrive in both temperate and warm shallow-marine environments. At most, it may have led to an expansion in their latitudinal distribution.

The siliciclastic influx in the Pyrenean Basin during the PETM, which increased sedimentation rates by a factor of two to five, is attributed to a significant seasonal intensification of the hydrological cycle within a generally drier climate (Schmitz et al. 2001; Schmitz and Pujalte 2007; Payros et al. 2022). Supporting this conclusion, modelling by Cecil and Dulong (2003) found that fluvial erosion and sediment loads increase under highly seasonal precipitation ranging from 300 to 600 mm per year. A recent instance of this relationship was observed in eastern Spain on 29 October 2024, when a prolonged dry spell was abruptly interrupted by rainfall exceeding the total annual average in less than two days, causing a catastrophic flooding. As a result, the area was blanketed with tons of mud.

The massive influx of terrestrial siliciclastic sediments into the Pyrenean Basin, particularly muds, must have had a significant impact on biotic communities. Larger foraminifera flourish under stable oligotrophic conditions and are recognised as K-strategists (Hottinger 1983, 1998). The influx

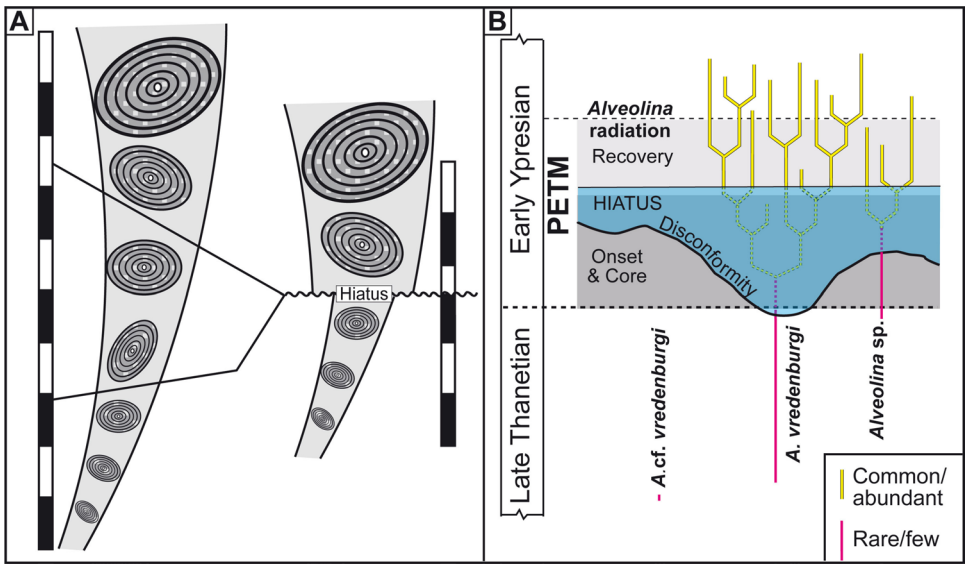

Fig. 12 **A** Simplified graph, inspired in Fig. 8 of Luterbacher (1998), illustrating how evolutionary lineages of larger foraminifera may be "telescoped" at unconformities and hiatal surfaces. **B** Alternative interpretation of the "Larger Foraminiferal Extinction and Origination event" (LFEO) described by Zhang et al. (2013) in the Tethys Himalaya, as an instance of telescoping at the hiatus associated with the disconformity between the core and recovery phases of the PETM

likely triggered seawater eutrophication, reduced water transparency and diminished light availability, thereby profoundly disrupting the habitat of larger foraminifera. The effects of these changes are exemplified by the fate of *Miscellanea*, a characteristic Palaeocene K-strategist. This larger foraminifer, which is abundant in the upper Thanetian of Campo (Scheibner et al. 2007), is absent from the PETM and lower Ypresian in this and other Pyrenean sections (Serra-Kiel et al. 2020). By contrast, *Nummulites* and *Alveolina* thrived during the PETM (Table 1), demonstrating a greater capacity than *Miscellanea* and other Paleocene larger foraminifera to adapt to the new environmental conditions brought about by the siliciclastic influx.

The case of lenticular *Nummulites* in the Urrobi section is particularly illustrative. In this section *Nummulites* first appear, scattered among lenticular and operculiniform *Assilina*, in the topmost 10 cm of the upper Thanetian carbonates (Fig. 6B, D). However, in the PETM Nummulites Band the situation is reversed, *Nummulites* overwhelmingly dominating the foraminiferal assemblage (Fig. 6E). A similar abrupt upsurge of *Nummulites* is observed in the Brecha de Arazas, Tozal del Cebollar and Tena sections (Fig. 4). A key question is whether a hiatus exists in the Urrobi section at the boundary between the Thanetian limestones and the Nummulites Band. Pujalte et al. (2003, their Fig. 5) concluded that the absence in Urrobi of the dissolution interval observed at Zumaia (Fig. S3B) might suggest a minor hiatus. If this were the case, it could be argued that the proliferation of *Nummulites* in the PETM mudstones was partly due to a telescoping effect. However, as noted above, the acidification of shallow-marine waters during the PETM (and thus $CaCO_3$ dissolution) was either weak or absent, which undermines this argument.

Paradoxically, data from the Basque Basin support the absence of both a hiatus and any telescoping effect at Urrobi. Thanetian deep-sea successions in the Basque Basin are typically capped by a hemipelagic greenish limestone, up to 60 cm thick ("Green Limestone" in Figs. S3B, S6A, B), its distinctive colour due to the glauconite infilling of planktonic foraminifera tests. In Zumaia, where no evidence of a hiatus is observed, the onset of the PETM occurs within a thin marly interval that overlies this limestone (Fig. S3B). Both the Green Limestone and the overlying marly interval are also present in Ermua, although with several intercalated turbidites (Fig. 7B). Notably, some of the turbidites within the PETM onset and core contain lenticular *Nummulites* (Fig. 7B, C). While these specimens are clearly resedimented, their presence indicates that *Nummulites* were flourishing on the mid-platform from the very onset of the PETM.

The appearance pattern of *Alveolina* mirrors that of *Nummulites*. Its first Pyrenean occurrence was found in uppermost Thanetian limestones, although so far only in the Korres section (Fig. 5). These limestones became subaerially exposed during the PETM due to a late Thanetian sea-level fall, as shown by their capping karstified surface and the overlying terrestrial mudstones. Subsequently, the section was reflooded during the Ilerdian transgression, and *Alveolina* became abundant and diverse, a clear example of telescoping (Fig. 5). However, during the PETM *Alveolina* specimens are already abundant in the Brecha de Arazas and Tozal del Cebollar sections (Fig. 4, Table 1). Sedimentological evidence shows that these specimens were transported by storm return currents, but their presence implies a significant proliferation in shallow waters during the PETM. The subsequent extensive development of the *Alveolina* Limestone Formation provides clear evidence that, in inner-platform settings, *Alveolina* came to dominate the foraminiferal assemblage during the early Ypresian.

It can thus be concluded that what characterised the LFT in the Pyrenean Basin was not the first appearance of *Nummulites* and *Alveolina*, but their sudden proliferation during the PETM. This proliferation was driven by the eutrophication caused by a massive siliciclastic influx, which was far more voluminous than in the Tethys. It is therefore hardly surprising that this turnover was first identified in the Pyrenees (Hottinger and Schaub 1960).

Impact of the PETM on larger foraminifera in the Tethys and in the Limalok Guyot

With some exceptions (e.g., Jiang et al. 2021), a substantial increase in terrigenous influx during the PETM is not observed in the Tethys realm. In fact, none of the sections from the Tethys considered here contain a siliciclastic intercalation within the PETM akin to that of the Pyrenees. However, Pogge von Strandmann et al. (2021) detected a negative lithium isotope excursion of ~ 3‰ in both global seawater (marine carbonates) and local weathering inputs (detrital shales), consistent with a substantial delivery of clays to the oceans. A global eutrophication of seawater during the PETM is also indicated by other proxies, including elevated biogenic barium values, used as a proxy for biological productivity (Schmitz et al. 1997b), and the deposition of black shales in sections from Egypt and Israel (Speijer and Wagner 2002). This eutrophication likely explains the correlation between the LFT and the PETM in the western Tethys sections of Slovenia and Egypt.

The impact of the PETM on larger foraminifera in the eastern Tethys requires a longer discussion, as published data are somewhat contradictory. Here, we summarize some of the interpretations from the eastern Tethys that diverge from those of the Pyrenean Basin and the western Tethys and propose explanations to reconcile the differences.

The main discrepancy concerns the origin of the LFT itself. Afzal et al. (2011) contended that the LFT was not

an instantaneous or synchronous event across the entire Tethyan region, solely induced by the PETM. Instead, they argued that it was a gradual process primarily driven by long-term evolutionary trends in larger foraminifera. Zhang et al. (2013) reinforced this perspective, suggesting that the LFT reflects natural evolutionary processes unrelated to the PETM. These conclusions appear to be based on the dissimilar occurrences of *Alveolina* and *Nummulites*, the most representative genera of the LFT.

In the Indus Basin of Pakistan, for example, occurrences of *Alveolina* are sparse, and *Nummulites* are absent (Afzal et al. 2011). Also, *A. vredenburgi* is recorded in sections of Pakistan at different horizons of the PETM, at the onset in Dularen, but in the middle part of its core in Nammal Gorge (Fig. 8C). However, it must be noted that, even in the Pyrenean Basin, *Alveolina* and *Nummulites* first appear at different levels of the PETM, depending on the depositional environment of the sections (Fig. 3B; Table 1). The diachrony in the Pakistan sections may be due to the same reason and therefore does not invalidate a causal relationship between the LFT and the PETM.

The occurrence of *A. vredenburgi* below the PETM in some Himalayan sections is perplexing (Fig. 9B). Its appearance ~ 65 m below the onset of the CIE in the ZP, ZM and F sections suggests that it predates the PETM by ~ 1.8 million years (assuming late Paleocene sedimentation rates were similar to those during the PETM). In the Zongpu section, *A.* cf. *vredenburgi* was identified at an even lower position, ~ 100 m below the PETM, although this was based on a single sample. In other sections, *A. vredenburgi* first appears at different levels. Notably, in sections where *Alveolina* is present below the PETM, its abundance remains consistently low (Fig. 9B). This, along with its absence in the Pakistani sections, suggests that *Alveolina* was rare and occupied limited ecological niches in the Lockhartia Sea during the late Thanetian. This situation, which persisted for nearly two million years, changed dramatically during the relatively brief PETM interval (~ 170 kyr; Röhl et al. 2007), when *Alveolina* became widespread and diversified. This challenges the interpretation of the LFT as a gradual process, instead reinforcing the PETM as its primary cause. Similarly, in the Pacific Ocean Limalok Guyot *Alveolina* was scarce below the PETM (with only two specimens), but abundant above it. It is also worth noticing that *Nummulites* appeared just above the PETM onset (Fig. 11).

A plausible explanation is that *Alveolina* originated in late Thanetian times in the tropical region of the Himalayan Tethys and/or the Pacific Ocean, but remained a minor component of the foraminiferal assemblage. According to Langer and Hottinger (2000), larger foraminifera disperse by rafting on algae, attaching to fish, and being transported while floating on marine currents. The westward-flowing surface current in the Tethys (Fig. 8A) likely facilitated their spread across the Tethys and into the Pyrenean Basin, although remaining a minor species. Their subsequent expansion in all zones, along with that of *Nummulites*, was triggered by the eutrophication induced by the PETM.

The so-called LFEO, first identified by Zhang et al. (2013), is another contentious issue. The event is characterized by the abrupt replacement, at a specific horizon during the PETM recovery, of Paleocene species with early Eocene species*, notably Alveolina* (Zhang et al. 2013, their Fig. 3). As previously indicated, however, the origin of this turnover has been attributed to both seawater eutrophication (Zhang et al. 2013, 2019) and environmental changes driven by a sea-level fall (Li et al. 2020). Here a third alternative is suggested, namely that the LFEO event represents a case of "telescoping" (Fig. 12B). This event, indeed, is associated with an erosional unconformity that caused a hiatus of variable magnitude (Zhang et al. 2019; Li et al. 2020). As a result, the core of the PETM is partly preserved in some sections, but it has been entirely removed in others (Figs. 10B, D). Interestingly, the *Alveolina* association above the unconformity is comparable, if not identical, to that of the radiation documented in the Pyrenees, which developed throughout the PETM. It is reasonable to assume that a similar evolution occurred in the eastern Tethys during the onset and core of the PETM, the record of which is missing at the hiatus (Fig. 12B).

A final discrepancy is the position of the onset of the CIE, the marker of the Paleocene-Eocene boundary, within the larger foraminifera zonation. There is a broad agreement in the Pyrenees, the western Tethys, and even in some eastern Tethys sections to place it at the SBZ4/SBZ5 transition. In contrast, Zhang et al. (2013, 2019) argued that, in the Himalayan Tibet, this boundary is situated in the upper part of SBZ5, based on the earlier first appearance of *A. vredenburgi* in some sections (e.g., Section 11 Mg at Gamba, Fig. 10A). This discrepancy also concerns the position of the base of the Ilerdian stage, which Hottinger (1998, his Fig. 1) aligned with the SBZ4/SBZ5 boundary. In the Pyrenean Basin, where the Ilerdian stage was defined, the precise location of the CIE in several sections made it evident that the lowest appearances of SBZ5 larger foraminifera occurred at different horizons (Fig. 3B, Table 1). To amend this chronostratigraphic issue, Pujalte et al. (2009) proposed redefining the base of the Ilerdian to make it coincide with the onset of the PETM. This proposal was contested by Zhang et al. (2013), who argued that the foundation of the Ilerdian stage was based, and should remain, on the evolutionary development of larger foraminifera.

The strict application of that biostratigraphic criterion, however, would lead to positioning the base of the Ilerdian at different chronostratigraphic levels in separate sections, both below and above the Paleocene–Eocene boundary (Table 1, Figs. 3B, 9B). Moreover, although most divisions

of the Geological Timescale were originally defined on biostratigraphic grounds, ongoing revisions using global stratotype-sections and points (GSSPs) in some places incorporate non-biostratigraphic markers, as is the case of the Paleocene–Eocene boundary (Aubry et al. 2007).

The data presented here demonstrate that the eutrophication associated with the PETM was the primary cause of the LFT in the Pyrenean Basin and throughout the Tethys Ocean. Establishing the base of the Ilerdian stage at the onset of the thermal event would stabilise its chronostratigraphic position, thereby rendering it globally valid. Furthermore, this approach would align the base of the Ilerdian with that of the standard Ypresian stage, simplifying the stratigraphic nomenclature.

Conclusions

The data presented in this paper conclusively demonstrate a genetic relationship between the PETM and the LFT, the event marking the base of the Ilerdian stage. In the Pyrenean Basin, the PETM significantly amplified the hydrological seasonal contrast of the early Paleogene semi-arid climate, greatly increasing the erosion and sediment load of the rivers flowing into the basin. Consequently, at least 14 km^3 of siliciclastic sand and nearly 100 km^3 of mud were introduced into the sea during the onset and core of the PETM. The massive influx of siliciclastics, particularly the mud, led to seawater eutrophication, reduced water transparency and diminished light availability, severely disrupting the habitat of larger foraminifera, which are K-strategists and thrive in stable, oligotrophic conditions. Some genera, such as *Miscellanea*, were significantly affected, while others, such as *Nummulites* and *Alveolina*, adapted to the changing conditions. Both genera were already present in the Pyrenean Basin just before the PETM, albeit scattered among late Thanetian species. However, they experienced an abrupt proliferation at the onset and core of the PETM, and by the recovery phase they radiated and diversified, becoming the dominant species of the larger foraminiferal community throughout the Eocene.

Most sections from the Tethys do not contain a similar intercalation of siliciclastic sediments at the PETM. However, lithium isotopes and other proxies indicate that eutrophication occurred throughout this ocean. In western Tethys sections, the LFT either coincides with the PETM onset or slightly postdates it. In the eastern Tethys, *Alveolina* and *Nummulites* became increasingly abundant during the PETM, eventually replacing a Paleocene larger foraminiferal assemblage rich in *Lockhartia*. Their first appearance in sections of Pakistan is slightly diachronous across the thermal event, whereas in Himalayan sections *A. vredenburgi* has been documented in the Thanetian, more than 1.8 Myr before the PETM. These facts have led some authors to question a genetic relationship between the LFT and the PETM. However, the diachrony in Pakistan is likely an artefact resulting from environmental factors. In the Himalayas, *A. vredenburgi* was a minor species during the Thanetian but radiated rapidly during the comparatively brief PETM interval (170 kyr), when *Nummulites* first appeared. Both observations support the notion that the PETM had a significant impact on the larger foraminiferal community across the entire Tethys Ocean.

The onset of the CIE/PETM is the official marker of the Palaeocene-Eocene boundary and the base of the standard Ypresian stage. Given the correlation between the LFT and the PETM, it makes sense to use the same criterion for the base of the regional Ilerdian stage.

Supplementary Information The online version contains supplementary material available at https://doi.org/10.1007/s10347-025-00709-1.

Acknowledgements Contribution to projects PID2019-105670GB-I00/AEI/10.13039/501100011033 (Spanish Government MCIU/AEI) and IT602-22 (Basque Government). NM-B had Margarita Salas funding (MARSA22/05, Spanish Government with EU Next Generation funds). This article benefited from insightful comments on a previous version of the manuscript by professors György Less and Maurice Tucker.

Funding Open Access funding provided thanks to the CRUE-CSIC agreement with Springer Nature. Agencia Estatal de Investigación, PID2019-105670 GB-I00/AEI/10.13039/501100011033, Aitor Payros, Eusko Jaurlaritza, IT602-22, Aitor Payros

References

Abd-Elhameed S, Mahmoud AA, Salama Y (2023) Late Paleocene-Early Eocene larger foraminifera from the Galala Plateaus, North Eastern Desert, Egypt: biostratigraphic, paleoenvironmental and paleoecological implications. Carbonates Evaporites 38:84. https://doi.org/10.1007/s13146-023-00909-2

Afzal J, Williams M, Leng MJ, Aldridge RJ, Stephenson MH (2011) Evolution of Paleocene to Early Eocene larger benthic foraminifer assemblages of the Indus Basin, Pakistan. Lethaia 44:299–320. https://doi.org/10.1111/j.1502-3931.2010.00247.x

Alegret L, Ortiz S, Orue-Etxebarria X, Bernaola G, Baceta JI, Monechi S, Apellaniz E, Pujalte V (2009) The Paleocene-Eocene thermal maximum: new data on microfossil turnover at the Zumaia

section, Spain. Palaios 24:318–328. https://doi.org/10.2110/palo.2008.p08-057r

Ali M, Coletti G, Garzanti E, Adatte T, Castelltort S, Sternai P, Benedetti A, Malinverno E, Luca Mariani L, Spangenberg JE, Khan S, Basso D, Samankassou E, Kocsis L, Usman M (2025) The Baroch Nala section (NE Pakistan): a new PETM standard for the eastern Tethys. Mar Pet Geol 171:107183. https://doi.org/10.1016/j.marpetgeo.2024.107183

Aubry MP, Ouda K, Dupuis C, Berggren WA, Van Couvering JA, Ali J, Brinkhuis H, Gingerich PD, Heilmann-Clausen C, Hooker J, Kent DV, King C, Knox RWO'B, Laga P, Molina E, Schmitz B, Steurbaut E, Ward DR, (2007) The global standard stratotype-section and point (GSSP) for the base of the Eocene series in the Dababiya section (Egypt). Episodes 30:271–286. https://doi.org/10.18814/epiiugs/2007/v30i4/003

Baceta JI, Pujalte V, Serra-Kiel J, Robador A, Orue-Etxebarria X (2004) El Maastrichtiense final, Paleoceno e Ilerdiense inferior de la Cordillera Pirenaica. In: Vera JA (ed) Geología de España. Sociedad Geológica de España, Instituto Geológico y Minero de España, Madrid, pp 308–313 (**In Spanish**)

Baceta J, Pujalte V, Wright VP, Schmitz B (2011) Carbonate platform models, sea-level changes and extreme climatic events during the Paleocene-early Eocene greenhouse interval: a basin-platform-coastal plain transect across the southern Pyrenean basin. In: Arenas C, Pomar L, Colombo L (eds). Pree-meeting Field trips Guidebook, 28th IAS meeting, Zaragoza. (Sociedad Geológica de España, Madrid, Geo-Guías. pp 151–198

Baceta JI (1996) El Maastrichtiense superior, Paleoceno e Ilerdiense inferior de la Región Vasco-Cantábrica: secuencias deposicionales, facies y evolución paleogeográfica. PhD thesis, University of the Basque Country (In Spanish)

Bassi D (2014) Rotaliid shell architecture and the Palaeodiversity of the Lockhartia sea. In: Hottinger L, Bassi D (eds) Paleogene larger rotaliid foraminifera from the western and central neotethys. Springer International Publishing, Cham, pp 3–12

Beasley C, Cotton L, Al-Suwaidi A, LeVay L, Sluijs A, Ullmann CV, Hesselbo S, Kate Little K (2021) Triumph and tribulation for shallow water fauna during the Paleocene-Eocene transition; insights from the United Arab Emirates. Newsl Stratigr 54:79–106. https://doi.org/10.1127/nos/2020/0573

Bolle MP, Adatte T, Keller G, von Salis K, Hunziker J (1998) Biostratigraphy, mineralogy and geochemistry of the Trabakua Pass and Ermua sections in Spain: Paleocene-Eocene transition. Eclog Geol Helv 91:1–25. https://doi.org/10.5169/seals-168405

Cecil CB, Dulong FT (2003) Precipitation models for sediment supply in warm climates. Soc Sediment Geol Spec Publ 77:21–27. https://doi.org/10.2110/pec.03.77.0021

Dinarès-Turell J, Baceta JI, Pujalte V, Orue-Etxebarria X, Bernaola G (2002) Magnetostratigraphic and cyclostratigraphic calibration of a prospective Palaeocene/Eocene stratotype at Zumaia (Basque Basin, northern Spain). Terra Nova 14:371–378. https://doi.org/10.1046/j.1365-3121.2002.00431.x

Gibbs SJ, Bown PR, Sessa JA, Bralower TJ, Wilson PA (2006) Nannoplankton extinction and origination across the Paleocene-Eocene thermal maximum. Science 314:1770–1773. https://doi.org/10.1126/science.1133902

Gingerich PD (2003) Mammalian responses to climate change at the Paleocene-Eocene boundary: Polecat Bench record in the northern Bighorn Basin, Wyoming. Geol Soc Am Spec Pap 369:463–478. https://doi.org/10.1130/0-8137-2369-8.463

Hamon Y, Deschamps R, Joseph P, Doligez B, Schmitz J, Lerat O (2016) Integrated workflow for characterization and modelling of a mixed sedimentary system: the Ilerdian Alveolina Limestone Formation (Early Eocene, Graus-Tremp Basin, Pyrenees, Spain). C R Geoscience 348:520–530. https://doi.org/10.1016/j.crte.2015.07.002

Hanif M, Sabba M, Ali N, Rahman MU, Ali F, Swati MAF (2021) A multi-proxy based high-resolution stratigraphical analysis of the possible Palaeocene-Eocene boundary interval, Salt Range, Pakistan. Geol J 56:434–456. https://doi.org/10.1002/gj.3912

Haq BU (1981) Paleogene paleoceanography: early Cenozoic oceans revisited. Oceanol Acta 4:71–82

Hottinger L (1983) Processes determining the distribution of larger foraminifera in space and time. Utrecht Micropaleont Bull 30:239–253

Hottinger L (1998) Shallow benthic foraminifera at the Paleocene-Eocene boundary. Strata 9:61–64

Hottinger L, Schaub H (1960) Zur Stufeneinteilung des Paleocaens und Eocaens: Einführung der stufer Ilerdien und Biarritzien. Eclog Geol Helv 53:454–479

Jiang J, Hu X, Li J, BouDagher-Fadel M, Garzanti E (2021) Discovery of the Paleocene-Eocene Thermal Maximum in shallow-marine sediments of the Xigaze forearc basin, Tibet: a record of enhanced extreme precipitation and siliciclastic sediment flux. Palaeogeogr Palaeoclimatol Palaeoecol 562:110095. https://doi.org/10.1016/j.palaeo.2020.110095

Kaiho K, Takeda K, Petrizzo MR, Zachos JC (2006) Anomalous shifts in tropical Pacific planktonic and benthic foraminiferal test size during the Paleocene-Eocene thermal maximum. Palaeogeogr Palaeoclimatol Palaeoecol 237:456–464. https://doi.org/10.1016/j.palaeo.2005.12.017

Kamran M, Frontalini F, Xi D, Papazzoni CA, Jafarian A, Latif K, Jiang T, Mirz K, Song H, Wan X (2021) Larger benthic foraminiferal response to the PETM in the Potwar Basin (Eastern Neotethys, Pakistan). Palaeogeogr Palaeoclimatol Palaeoecol 575:110450. https://doi.org/10.1016/j.palaeo.2021.110450

Langer MR, Hottinger L (2000) Biogeography of selected "larger" foraminifera. Micropaleontol 46:105–126

Li J, Hu X, Garzanti E, BouDagher-Fadel M (2017) Shallow-water carbonate responses to the Paleocene-Eocene thermal maximum in the Tethyan Himalaya (southern Tibet): Tectonic and climatic implications. Palaeogeogr Palaeoclimatol Palaeoecol 466:153–165. https://doi.org/10.1016/j.palaeo.2016.11.026

Li J, Hu X, Zachos JC, Garzanti E, BouDagher-Fadel M (2020) Sea level, biotic and carbon-isotope response to the Palaeocene-Eocene thermal maximum in Tibetan Himalayan platform carbonates. Glob Planet Change 194:103316. https://doi.org/10.1016/j.gloplacha.2020.103316

Luterbacher HP (1998) Sequence stratigraphy and the limitations of biostratigraphy in the marine Paleogene strata of the Tremp basin (central part of the southern Pyrenean foreland basin, Spain). In: de Gracianski PC, Hardenbol J, Jacquin T, Vail PR (eds) Mesozoic and Cenozoic Sequence Stratigraphy of European Basins. SEPM Spec Publ, pp 303–309

Luterbacher HP (1973) La sección tipo del Piso Ilerdiense. In: Unknown editors (eds) Guidebook of the XIII Coloquio Europeo de Micropaleontología, ENADIMSA, Madrid, pp 113–140 (**in Spanish**)

Manners HR, Grimes ST, Sutton PA, Domingo L, Leng MJ, Twitchett RJ, Hart MB, Dunkley Jones T, Pancost RD, Duller R, Lopez-Martinez N (2013) Magnitude and profile of organic carbon isotope records from the Paleocene–EoceneThermal Maximum: evidence from northern Spain. Earth Planet Sci Lett 376:220–230. https://doi.org/10.1016/j.epsl.2013.06.016

Martínez-Braceras N, Franceschetti G, Payros A, Monechi S, Dinarès-Turell J (2023) High-resolution cyclochronology of the lowermost Ypresian Arnakatxa section (Basque-Cantabrian basin, western Pyrenees). Newslett Strat 56:53–74. https://doi.org/10.1127/nos/2022/0706

Martín-Martín M, Guerrera F, Tosquella J, Tramontana M (2020) Paleocene-lower Eocene carbonate platforms of westernmost Tethys. Sediment Geol 404:105674. https://doi.org/10.1016/j.sedgeo.2020.105674

McInerney FA, Wing SL (2011) The Paleocene-Eocene thermal maximum: a perturbation of carbon cycle, climate, and biosphere with implications for the future. Ann Rev Earth Plan Sci 39:489–516. https://doi.org/10.1146/annurev-earth-040610-133431

Mutti E, Seguret M, Sgavetti M (1988) Sedimentation and deformation in the tertiary sequences of the southern Pyrenees. AAPG Mediterranean Basins Conf, Nice, Field Trip Guide, p 7

Nicora A, Premoli Silva I, Arnaud Vanneau A (1995) Paleogene larger foraminifer biostratigraphy from Limalok Guyot, Site 871. In: Haggerty JA, Premoli Silva I, Rack F, McNutt MK (eds) Proceedings of the Ocean Drilling Program, Scientific results, vol. 144, pp 127–139. https://doi.org/10.2973/odp.proc.sr.144.012.1995

Nuñez-Betelu L, Baceta JI (1994) Basics and application of rock-Eval/TOC pyrolysis: an example from the uppermost Paleocene/lowermost Eocene in The Basque Basin, Western Pyrenees. Munibe 46:43–62

Orue-Etxebarria X, Apellaniz E, Baceta JI, Coccioni R, Di Leo R, Dinarès-Turell J, Galeotti S, Monechi S, Núñez-Betelu K, Parés JM, Payros A, Pujalte V, Samsó JM, Serra-Kie J, Schmitz B, Tosquella J (1996) Physical and biostratigraphic analysis of two prospective Paleocene-Eocene Boundary stratotypes in the intermediate-deep water Basque Basin, western Pyrenees: the Trabakua Pass and Ermua sections. Neues Jahrb Geol Paläontol Abh 201:179–242

Orue-Etxebarria X, Pujalte V, Bernaola G, Apellaniz E, Baceta JI, Payros A, Nunez-Betelu K, Serra-Kiel J, Tosquella J (2001) Did the late Paleocene termal maximum affect the evolution of larger foraminifers? Evidence from calcareous plankton of the Campo Section (Pyrenees, Spain). Mar Micropaleontol 41:45–71. https://doi.org/10.1016/S0377-8398(00)00052-9

Orue-Etxebarria X, Bernaola G, Baceta JI, Angori E, Caballero F, Monechi S, Pujalte V, Dinarès-Turell J, Apellaniz E, Payros A (2004) New constraints on the evolution of planktic foraminifera and calcareous nannofossils across the Paleocene-Eocene boundary interval: the Zumaia section revisited. Neues Jahrb Geol Paläontol Abh 234:223–259

Payros A, Pujalte V, Schmitz B (2022) Mid-latitude alluvial and hydroclimatic changes during the Paleocene-Eocene thermal maximum as recorded in the Tremp-Graus Basin. Spain Sedim Geol 435:106155. https://doi.org/10.1016/j.sedgeo.2022.106155

Petrizzo MR (2007) The onset of the Paleocene-Eocene thermal maximum (PETM) at sites 1209 and 1210 (Shatsky Rise, Pacific Ocean) as recorded by planktonic foraminifera. Mar Micropaleontol 63:187–200. https://doi.org/10.1016/j.marmicro.2006.11.007

Plaziat JC (1981) Late cretaceous to Late Eocene palaeogeographic evolution of southwest Europe. Palaeogeogr Palaeoclimatol Palaeoecol 36:263–320. https://doi.org/10.1016/0031-0182(81)90110-3

Premoli Silva I, Haggerty J, Rack F, and the Shipboard Scientific Party (1993) Northwest Pacific atolls and guyots: Sites 871–880 and Site 801. Proceedings of the Ocean Drilling Program Initial reports 144. College Station, Texas. https://doi.org/10.2973/odp.proc.ir.144.1993

Pujalte V, Baceta JI, Apellaniz E, Orue-Etxebarria X, PayrosA S-K (1998) An early Ilerdian transient switch-off in shallow and deep-water carbonate deposition in the western Pyrenees, Spain. Strata 9:111–112

Pujalte V, Baceta JI, Schmitz B, Orue-Etxebarria X, Payros A, Bernaola G, Apellaniz E, Caballero F, Robador A, Serra-Kiel J, Tosquella J (2009) Redefinition of the Ilerdian Stage (early Eocene). Geol Acta 7:177–194. https://doi.org/10.1344/105.000000268

Pujalte V, Baceta JI, Schmitz B (2015) A massive input of coarse-grained siliciclastics in the Pyrenean Basin during the PETM: the missing ingredient in a coeval abrupt change in hydrological regime. Clim past 11:1653–1672. https://doi.org/10.5194/cp-11-1653-2015

Pujalte V, Robador A, Payros A, Samsó JM (2016) A siliciclastic braid delta within a lower Paleogene carbonate platform (Ordesa-Monte Perdido national park, southern Pyrenees, Spain): record of the Paleocene-Eocene thermal maximum perturbation. Palaeogeogr Palaeoclimatol Palaeoecol 459:453–470. https://doi.org/10.1016/j.palaeo.2016.07.029

Pujalte V, Schmitz B, Payros A (2022) A rapid sedimentary response to the Paleocene-Eocene thermal maximum hydrological change: new data from alluvial units of the Tremp-Graus basin (Spanish Pyrenees). Palaeogeogr Palaeoclimatol Palaeoecol 589:110818. https://doi.org/10.1016/j.palaeo.2021.110818

Pujalte V, Orue-Etxebarria X, Schmitz B, Tosquella J, Baceta JI, Payros A, Bernaola G, Caballero F, Apellani, E (2003) Basal Ilerdian (earliest Eocene) turnover of larger foraminifera: age constraints based on calcareous plankton and $\delta^{13}C$ isotopic profiles from new southern Pyrenean sections (Spain). In: Wing SL, Gingerich PD, Schmitz B, Thomas E (eds) Causes and Consequences of Globally Warm Climates in the Early Paleogene. Geol Soc Am Spec Pap 369:205–221. https://doi.org/10.1130/0-8137-2369-8.205

Robador A, Samsó JM, Serra-Kiel J, Tosquella J (1991) Field guide. In: Barnolas A, Robador A, Serra-Kiel J, Caus E (eds) Introduction to the Early Paleogene of the south Pyrenean Basin, field-trip guidebook of the 1st meeting IGCP project 286. Inst Tecno Geomin España, Madrid, pp 131–159

Robador A (2008) El Paleoceno e Ilerdiense inferior del Pirineo occidental: Estratigrafía y Sedimentología. PhD Thesis University of the Basque Country. Publicaciones del Instituto Geológico y Minero de España, Madrid, Serie Tesis Doctorales 12 (In Spanish)

Robinson SA (2011) Shallow-water carbonate record of the Paleocene-Eocene thermal maximum from a pacific ocean guyot. Geology 39:51–54. https://doi.org/10.1130/G31422.1

Röhl U, Westerhold T, Bralower TJ, Zachos JC (2007) On the duration of the Paleocene-Eocene thermal maximum (PETM). Geochem Geophys Geosyst 8:12. https://doi.org/10.1029/2007GC001784

Schaub H (1973) La sección de Campo (provincia de Huesca). In: Unknown editors (eds) Guidebook of the XIII Coloquio Europeo de Micropaleontología, ENADIMSA, Madrid, pp 151–170 (**in Spanish**)

Schaub H (1981) *Nummulites* et *Assilines* de la Téthys Paléogène: Taxinomie, phylogénesè et biostratigraphie: Mémoires Suisses de Paléontologie 104–106:1–236

Scheibner C, Speijer RP (2009) Recalibration of the Tethyan shallow-benthic zonation across the Paleocene-Eocene boundary: the Egyptian record. Geol Acta 7:195–214. https://doi.org/10.1344/105.000000267

Scheibner C, Speijer RP, Marzouk AM (2005) Turnover of larger Foraminifera during the Paleocene-Eocene thermal maximum and paleoclimatic control on the evolution of platform ecosystems. Geology 33:493–496. https://doi.org/10.1130/G21237.1

Scheibner C, Rasser MW, M, Mutti M, (2007) The Campo section (Pyrenees, Spain) revisited: Implications for changing benthic carbonate assemblages across the Paleocene-Eocene boundary. Palaeogeogr Palaeoclimatol Palaeoecol 248:145–168. https://doi.org/10.1016/j.palaeo.2006.12.007

Schmitz B, Pujalte V (2003) Sea-level, humidity, and land-erosion records across the initial Eocene thermal maximum from a continental-marine transect in northern Spain. Geology 31:689–692. https://doi.org/10.1130/G19527.1

Schmitz B, Pujalte V (2007) Abrupt increase in seasonal extreme precipitation at the Paleocene-Eocene boundary. Geology 35:215–218. https://doi.org/10.1130/G23261A.1

Schmitz B, Asaro F, Molina E, Monechi S, von Salis K, Speijer RP (1997a) High-resolution iridium, δ^3C, δ^8O, foraminifera and nannofossil profiles across the latest Paleocene benthic extinction event at Zumaya, Spain. Palaeogeogr Palaeoclimatol Palaeoecol 133:49–69. https://doi.org/10.1016/S0031-0182(97)00024-2

Schmitz B, Charisi SD, Thompson EI, Speijer RP (1997b) Barium, SiO_2 (excess), and P_2O_5 as proxies of biological productivity in the middle east during the Paleocene and the latest Paleocene benthic extinction event. Terra Nova 9:95–99. https://doi.org/10.1111/j.1365-3121.1997.tb00011.x

Schmitz B, Pujalte V, Núñez-Betelu K (2001) Climate and sea-level perturbations during the Incipient Eocene thermal Maximum: evidence from siliciclastic units in the Basque Basin (Ermua, Zumaia and Trabakua Pass), northern Spain. Palaeogeogr Palaeoclimatol Palaeoecol 165:299–320. https://doi.org/10.1016/S0031-0182(00)00167-X

Scotese CR (2010) Atlas of Paleogene paleogeographic maps (Mollweide projection). Evanston, Illinois

Serra-Kiel J, Canudo JI, Dinares J, Molina E, Ortiz N, Pascual JO, Samsó JM, Tosquella J (1994) Cronoestratigrafía de los sedimentos marinos del Terciario inferior de la Cuenca de Graus-Tremp (Zona Central Surpirenaica). Rev Soc Geol España 7:273–297 (**in Spanish**)

Serra-Kiel J, Vicedo V, Baceta JI, Bernaola G, Robador A (2020) Paleocene larger foraminifera from the Pyrenean Basin with a recalibration of the Paleocene shallow benthic zones. Geol Acta 18:1–69. https://doi.org/10.1344/GeologicaActa2020.18.8

Speijer RP, Wagner R (2002) Sea-level changes and black shales associated with the late Paleocene thermal maximum: Organic-geochemical and micropaleontologic evidence from the southern Tethyan margin (Egypt-Israel). In: MacLeod KG, Koeberl C (eds) Catastrophic events and mass extinctions: Impacts and beyond. Geol Soc Am Spec Pap, pp 533–549

Speijer RP, Pälike H, Hollis CJ, Hooker JJ, Ogg JG (2020) Chapter 28—The Paleogene period. In: Gradstein FM, Ogg JG, Schmitz MD, Ogg GM (eds) Geologic Time Scale 2020. Elsevier, Amsterdam, pp 1087–1140

Storme JY, Devleeschouwer X, Schnyder J, Cambier G, Baceta JI, Pujalte V, Di Matteo A, Iacumin P, Yans J (2012) The Palaeocene/Eocene boundary section at Zumaia (Basque-Cantabric Basin) revisited: new insights from high-resolution magnetic susceptibility and carbon isotope chemostratigraphy on organic matter ($\delta^{13}Corg$). Terra Nova 24:310–317. https://doi.org/10.1111/j.1365-3121.2012.01064.x

Thomas E (2007) Cenozoic mass extinctions in the deep sea: What perturbs the largest habitat on Earth? Geol Soc Am Spec Pap 424:1–23. https://doi.org/10.1130/2007.2424(01)

Van Wagoner JC, Posamentier HW, Mitchum RM, Vail PR, Sarg JF, Loutit TS, Hardenbol J (1988) An overview of the fundamentals of sequence stratigraphy and key definitions. In: Posamentier HW, Ross CA, Van Wagoner JC, Wilgus JC, Hastings BS, Kendall CGStC (eds) Sea-Level Changes: An Integrated Approach. Soc Econ Paleontol Mineral Spec Publ, pp 39–45

Vandenberghe N, Hilgen FJ, Speijer RP (2012) The Paleogene period. In: Gradstein FM, Ogg JG, Schmitz MD, Ogg GM (eds) The Geological Timescale 2012. Elsevier, Amterdam, pp 855–922

von Strandmann P, PhAE JMT, Joshua West A, Murphy MJ, Stokke EW, Tarbuck G, Wilson DJ, Pearce ChR, Schmidt DN (2021) Lithium isotope evidence for enhanced weathering and erosion during the Paleocene-Eocene thermal maximum. Sci Adv 7:eabh4224. https://doi.org/10.1126/sciadv.abh4224

Zachos JC, Rohl U, Schellenberg SA, Sluijs A, Hodell DA, Kelly DC, Thomas E, Nicolo M, Raffi I, Lourens LJ, McCarren H, Kroon D (2005) Rapid acidification of the ocean during the Paleocene-Eocene thermal maximum. Science 308:1611–1615. https://doi.org/10.1126/science.1109004

Zamagni J, Mutti M, Ballato P, Kosir A (2012) The Paleocene-Eocene thermal maximum (PETM) in shallow-marine successions of the Adriatic carbonate platform (SW Slovenia). Geol Soc Am Bull 124:1071−1086

Zhang Q, Willems H, Ding L (2013) Evolution of the Paleocene-Early Eocene larger benthic foraminifera in the Tethyan Himalaya of Tibet, China. Int J Earth Sci 102:1427–1445. https://doi.org/10.1007/s00531-012-0856-2

Zhang Q, Willems H, Ding L, Xu X (2019) Response of larger benthic foraminifera to the Paleocene-Eocene thermal maximum and the position of the Paleocene/Eocene boundary in the Tethyan shallow benthic zones: evidence from South Tibet. Geol Soc Am Bull 131:84–98. https://doi.org/10.1130/B31813.1